Chapter 14

Weak Quasielastic $\nu\left(\bar{\nu}\right)$-nucleus Scattering

14.1 Introduction

In Chapters 10–13, we have discussed (anti)neutrino interactions on the free nucleon target leading to quasielastic (Chapter 10), inelastic (Chapters 11 and 12), and deep inelastic scattering (Chapters 13) depending upon the energy transferred to the target and the four-momentum transfer squared. The study of such processes is important to understand the various basic weak interaction processes induced by (anti)neutrinos from the free nucleons and determine the quasielastic form factors, transition form factors, and the structure functions of the nucleon at the $WNN(ZNN)$ vertex. In recent times, the study of (anti)neutrino reactions from the nuclear targets has been emphasized as almost all the present generation (anti)neutrino experiments use moderate to heavy nuclear targets like ^{12}C, ^{16}O, ^{40}Ar, ^{56}Fe, ^{208}Pb, where the interactions take place with the nucleons that are bound inside the nucleus. Various experiments like MINERvA, NOvA, T2K, etc., are being performed in the few GeV energy region where the contribution to the scattering cross section comes from all the possible channels, viz., quasielastic, inelastic, and deep inelastic scattering processes. A good understanding of the nuclear cross sections would be very helpful in analyzing these experiments. The precision with which the basic neutrino–nucleon cross sections in nuclear targets are known is still not better than 20–30%.

Neutrino oscillation experiments measure events that are a convolution of

(i) energy-dependent neutrino flux and

(ii) energy-dependent cross section.

Moreover, the nuclear medium effects modulating the cross sections are energy dependent. Therefore, it is highly desirable that we understand the energy dependence of nuclear medium effects in neutrino scattering processes; this understanding will help in achieving the future goals of physicists involved in studying CP violation and the mass hierarchy problem in the phenomenology of neutrino oscillations (Chapter 18).

https://doi.org/10.1017/9781108489065.015 Published online by Cambridge University Press

Broadly, we may divide nuclear processes induced by neutrinos into two categories. The first one is the exclusive reactions

$$\nu_l(k) \; + \; {}^{A}_{Z_i}X(p) \; \rightarrow \; l^-(k') \; + \; {}^{A}_{Z_f}Y(p'), \tag{14.1}$$

where $Z_i(Z_f)$ is the charge of initial (final) nucleus. In this case, the final nucleus ${}^{A}_{Z_f}Y$ is left either in the ground state or in an excited state, which decays into some final nuclear states through electromagnetic or weak interactions by emitting photons or charged leptons which are observed. The second is the inclusive reaction in which only the leptons produced through the charged current reactions are observed and no observation is made on the hadrons or nuclei produced in the reaction. In the case of inclusive quasielastic reactions, the kinematics of the final lepton is used to ascertain the quasielastic nature of the reaction. In this chapter, we will discuss nuclear medium effects in quasielastic scattering processes; and the nuclear medium effects in inelastic and deep inelastic scattering processes will be discussed in Chapters 15 and 16 respectively.

In the region of very low energy relevant for reactor and solar neutrinos (Chapter 17), the exclusive transitions to the ground state or a few low excited states in the final nucleus are accessible. However, in the region of intermediate and high energies relevant to atmospheric and accelerator neutrinos, inclusive reactions are the most relevant processes. In this energy region, in addition to the quasielastic scattering, other neutrino processes are also very important as shown in Figure 14.1, where the total scattering cross section per nucleon per unit energy of the incoming neutrino and antineutrino in the charged current sector is presented as a function of the neutrino energy. The individual contributions to the quasielastic, inelastic, and deep inelastic scattering cross section as well as the sum of all the processes are shown and compared with the available experimental data. It is evident from the figure that in the few GeV energy region all the three processes, viz., quasielastic, inelastic, and deep inelastic scattering, have significant contributions in the neutrino and antineutrino induced processes. It may be noticed that the quasielastic scattering cross sections per unit energy peaks at $\sim$0.3 GeV while its contribution is non-negligible even at high energies. Inelastic scattering is very important in the $\sim 1-3$ GeV energy region as it dominates over the quasielastic and DIS processes, although the peak lies at $\sim$2 GeV. In the Deep Underground Neutrino Experiment (DUNE), it is expected that more than 30% of the events would come from the DIS region and 50% of the events would come through the nonresonant and resonant production of mesons also known as the shallow inelastic region and the DIS region. The onset for the DIS process is considered to be $\sim$2 GeV and the cross section in this region increases almost linearly with the increase in the neutrino energy up to $E_{\nu_l} \approx 100$ GeV. Moreover, it may be observed from the figure that the experimental data have large error bars. Presently, the ongoing and planned experiments are trying to obtain high statistics data with better precision.

The charged current neutrino and antineutrino induced quasielastic inclusive reactions are expressed as

$$\nu_l(k) \; + \; {}^{A}_{Z}Y(p) \; \rightarrow \; l^-(k') \; + \; X(p'), \tag{14.2}$$

$$\bar{\nu_l}(k) \; + \; {}^{A}_{Z}Y(p) \; \rightarrow \; l^+(k') \; + \; X(p'), \tag{14.3}$$

https://doi.org/10.1017/9781108489065.015 Published online by Cambridge University Press

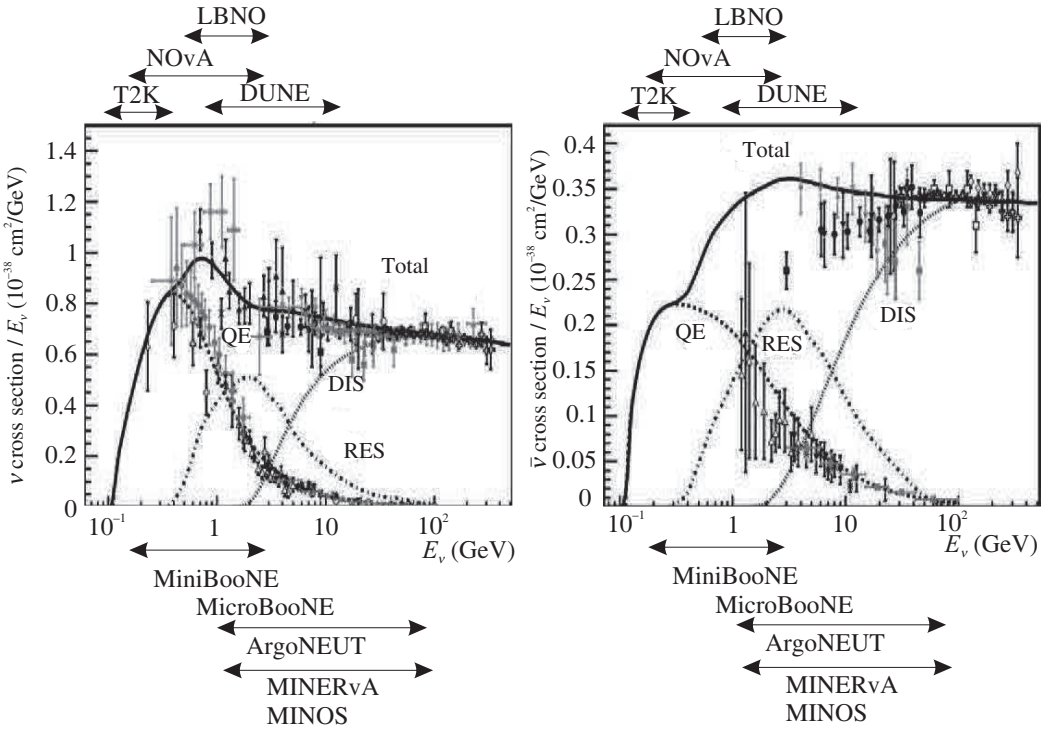

Figure 14.1 Charged current induced total scattering cross section per nucleon per unit energy of the incoming particles vs. neutrino (left panel) and antineutrino (right panel) energy. The dashed line shows the contribution from the quasielastic (QE) scattering while the dashed-dotted and dotted lines represent the contributions from the inelastic resonance (RES) and deep inelastic scattering (DIS), respectively. The sum of all the scattering cross sections (TOTAL) is shown by the solid line [630].

in which a neutrino or antineutrino scatters from a nucleon inside the nucleus. X stands for the hadronic debris produced in inclusive inelastic scattering.

The quasielastic scattering of neutrinos and antineutrinos from the nuclear targets in the entire region from low energy to very high energy has been the focus of extensive theoretical and experimental work for more than 50 years. In the very low energy region of few MeV, the QE reactions on nuclei are relevant for the astrophysical and reactor (anti)neutrinos while in the intermediate energy region of $E_{\nu(\bar{\nu})} \leq 5$ GeV, they are relevant for the accelerator and atmospheric neutrinos. While the nuclear effects are known to play an important role in the low energy region of QE scattering, it has been surprising and unexpected to see the effect of the nuclear medium even at very high energy in the region of deep inelastic scattering revealed through the EMC (European Muon Collaboration) effect (Chapter 16).

Historically, the first experiments on quasielastic $\nu(\bar{\nu})$ reactions from nuclear targets using reactor (anti)neutrinos were proposed by Pontecorvo [80]; and with the accelerator neutrinos by Pontecorvo [105], Schwartz [106], and Markov [631]. The early experiments with accelerator neutrinos were done with spark chambers (SC) on Al and Fe nuclei and with the bubble chambers (BC) on freon and propane [110, 156, 111, 385]. The early theoretical calculations for the quasielastic (anti)neutrino scattering from nuclei were done by Berman [632], Bell [633], Uberall [634], and Lovseth [635]. The primary aim of these reactions was to study the properties

https://doi.org/10.1017/9781108489065.015 Published online by Cambridge University Press

of (anti)neutrinos as well as the structure of the weak interaction theory at higher energy and high momentum transfers in order to understand the nucleon structure in the axial vector sector and to supplement our knowledge obtained from the electron scattering in the vector sector. In the mid-1970s, when the neutral current predicted by the standard model (Chapter 8) were discovered at CERN [636, 168], new interest was generated in studying the $\nu(\bar{\nu})$ reactions on nuclear targets induced by neutral currents. These nuclear reactions induced by charged and neutral weak currents had the advantage that the exclusive quasielastic reaction induced by neutrinos and antineutrinos to the specified nuclear states could be chosen to study each term in the neutral hadronic current according to the space time and isospin structure predicted by the standard model [637]. Various experiments to explore the structure of the neutral currents were done with the reactor and accelerator neutrinos and antineutrinos. Since then many experiments have been done in various laboratories around the world using other sources of neutrinos as well.

The discovery and study of the phenomenon of neutrino oscillations in atmospheric and solar neutrinos in the early 1990s, renewed the interest of the entire neutrino community in studying the quasielastic neutrino nucleus processes experimentally as well as theoretically, specially in the region of $E_{\nu(\bar{\nu})} \leq 2$ GeV. The phenomenology of neutrino oscillations (see Chapter 18) is determined by the (anti)neutrinos experiments done in the entire region of energy corresponding to the low, intermediate, and high energy to explore various parameters of neutrino oscillation phenomenology. In the low and intermediate energy region of (anti)neutrino reactions, the nuclear medium has considerable effect on various observables like the cross sections, angular, and energy distribution of the final lepton produced in QE reaction. Moreover, some inelastic channels in which hadrons like pions and correlated nucleons are produced could also give rise to QE-like signals through the reabsorption of pions and nucleons due to the final state interactions (FSI) which could take place in the nuclear medium. These nuclear medium effects are difficult to calculate and are model dependent. However, there are some basic nuclear medium effects which are easier to calculate and understand like the effects due to the binding energy, Fermi motion of the nucleon, and the aspects of nucleon–nucleon ($N - N$) correlations which could be described through the wave function of nucleus and determined using well-studied nucleon–nucleon interaction potentials. In view of the various types of the nucleon–nucleon potential studied in nuclear physics, there are many approaches developed in the literature to take into account the $N - N$ interaction and the nuclear wave functions for describing the quasielastic reactions of ν and $\bar{\nu}$ from the nuclear targets. In this chapter, we focus on the QE scattering of ν and $\bar{\nu}$ from the nuclear targets in the region of low and intermediate energies.

14.2 Physics of Nuclear Medium Effects in Quasielastic Scattering

There are two major ingredients to describe the QE $\nu(\bar{\nu})$ scattering from the nuclear targets:

(i) the theory of $\nu(\bar{\nu})$-nucleon scattering, and

(ii) the model to describe the nucleus.

https://doi.org/10.1017/9781108489065.015 Published online by Cambridge University Press

The former is described by the standard model (Chapter 10), while the latter has been studied extensively in the electron–nucleus and photon–nucleus reaction. In a simple picture, the (anti)neutrino scatters from a nucleon in which the scattering is induced by charged current (CC) interactions from a free nucleon at rest

$$\begin{aligned} \nu_l(k) + n(p) &\longrightarrow l^-(k') + p(p'), \\ \bar{\nu}_l(k) + p(p) &\longrightarrow l^+(k') + n(p'). \end{aligned} \tag{14.4}$$

The matrix element of this process can be written as

$$\mathcal{M} = \frac{G_F}{\sqrt{2}} \cos\theta_C \, l^\mu J_\mu, \tag{14.5}$$

where the leptonic current l_μ and the hadronic current are defined in Chapter 10.

Using this, we can write the matrix element squared averaged over the initial and summed over the final spins of the nucleon given by:

$$|\mathcal{M}|^2 = \frac{G_F^2}{2} \cos^2\theta_C \, L^{\mu\nu} J_{\mu\nu}. \tag{14.6}$$

The leptonic tensor $L^{\mu\nu}$ and the hadronic tensor $J_{\mu\nu}$ are given in Chapter 10 (section 10.5.3).

The differential scattering cross section can be expressed as

$$\frac{d^2\sigma_{\nu l}}{d\Omega(\hat{k}')dE_l'} = \frac{1}{E_n E_p} \frac{|\vec{k}'|}{|\vec{k}|} \frac{G_F^2 \cos^2\theta_C}{128\pi^2} \, L^{\mu\nu} J_{\mu\nu} \delta(E_\nu - E_l + E_n - E_p). \tag{14.7}$$

The energy momentum conservation for the reaction given in Eq. (14.4) implies that

$$(q+p)^2 = p'^2, \quad \text{where } q = k - k' = p' - p, \quad p^\mu = (M, \vec{0}), \tag{14.8}$$

leading to

$$q_0 = \Delta E = \frac{M'^2 - M^2 - q^2}{2M} \approx \frac{-q^2}{2M}. \tag{14.9}$$

It shows that the energy distribution of the final leptons would have a delta function peak at the aforementioned value of energy transfer $\Delta E = \frac{-q^2}{2M}$. However, in a nucleus, the nucleons are neither at rest nor non-interacting, leading to various types of nuclear effects of kinematical as well as dynamical origin. In the following, we describe them qualitatively and then discuss some of them quantitatively in later sections.

(i) **Nucleon binding**
The nucleons in the nucleus are bound and the binding energy of the nuclei is well studied and known. Consequently, the nucleons in the nuclei are off-mass shell and do not satisfy the energy momentum relation, that is, $p^2 = M^2$. There are many theoretical models suggesting that the effective mass of nucleons is reduced in the nuclear medium and the reduction is related to the strength of the potential responsible for the nuclear binding; it

https://doi.org/10.1017/9781108489065.015 Published online by Cambridge University Press

is therefore model dependent. In any case, this affects the free particle kinematics used in Eq. (14.9) and the peak of the energy distribution is shifted in the energy distribution of the nucleus around the peak corresponding to $\Delta E = \frac{-q^2}{2M}$.

(ii) **Fermi motion**

The nucleons in the nucleus move with a momentum $\vec{p}$. In the Fermi gas model, this momentum is bounded by a maximum momentum p_F called Fermi momentum given in terms of the density as

$$p_F = [3\pi^2\rho]^{\frac{1}{3}}, \tag{14.10}$$

ρ is the density of the nucleon in the nucleus.

In a shell model picture, the nucleons move in a central mean field described by a potential $V(r)$; the motion is described nonrelativistically by a Hamiltonian given by

$$H = -\frac{\vec{\nabla}^2}{2M} + V(r), \tag{14.11}$$

where $V(r)$ describes the mean field for which there are many models in the literature.

The momentum of the nucleon in a nucleus is then defined through the momentum distribution of the nucleons in the nuclei which is determined by the nucleon wave function $\psi(\vec{p})$ in momentum space obtained by solving the Schrodinger equation with H given in Eq. (14.11). This momentum distribution is called the spectral function of the nucleon $S(\vec{p}, E)$. In the simplest case of the Fermi gas model, it is given by:

$$S(\vec{p}, E) \propto \theta(p_F - p)\delta(E - \sqrt{|\vec{p}|^2 + M^2} + \epsilon), \tag{14.12}$$

where ϵ is the separation energy. In a realistic nucleus, the spectral function is related to $|\psi(\vec{p})|^2$. The cross sections from a nucleon of a given momentum $\vec{p}$ is then convoluted with the spectral function $S(\vec{p}, E)$.

Therefore, the elastic peak is not only shifted, but also smeared about the elastic peak depending upon the spectral function $S(\vec{p}, E)$. Historically, such smearing of the peak was observed in electron scattering and the process was called quasielastic elastic scattering (QEES).

(iii) **Pauli blocking**

In the conventional shell model picture of nuclei, various nuclear states are filled by neutrons and protons starting from the lowest possible state up to a certain nuclear state depending upon the number of nucleons. Similarly, in a Fermi gas picture of the nuclei, all the nuclear states in the Fermi sea are filled up to the momentum p_F (Figure 14.2), (a) and (b). This defines the ground state. In any nuclear reaction, the nucleons from a certain filled state are excited to a higher unoccupied state depending upon the energy transfer, creating a hole in the previously occupied state (Figure 14.2) (c). This is called

https://doi.org/10.1017/9781108489065.015 Published online by Cambridge University Press

the creation of a particle–hole $(1p-1h)$ state in the Hilbert space of nuclei or in the Fermi sea. Since the nucleons are fermions and follow Pauli's exclusion principle, the excited particles are not allowed to occupy the already filled states. Therefore, all the nuclear states up to a certain momentum in the phase space are inaccessible for occupation after scattering. This is called Pauli blocking and leads to the reduction in the cross section which could be substantial in certain kinematical regions especially in the region of low momentum transfers.

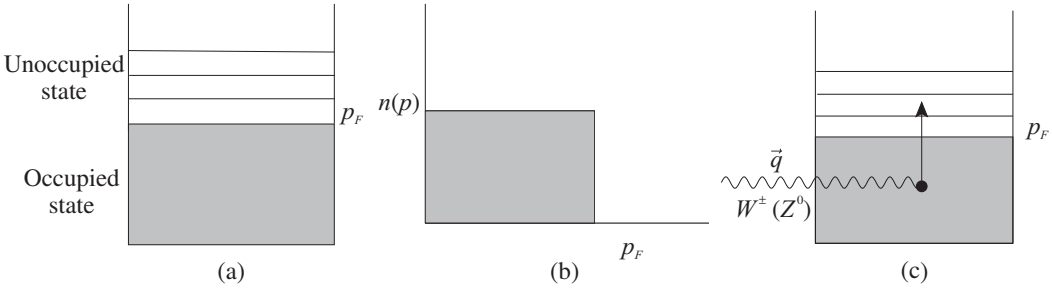

Figure 14.2 Diagrammatic representation of Pauli blocking.

(iv) **Meson exchange currents**

It has been established in the case of electromagnetic reactions induced by photons and electrons that in certain kinematical regions, external probes like photons and electrons interact with the mesons in flight while they are exchanged between nucleons in a nuclear medium as well as with non-nucleonic degrees of freedom like Δ in nuclei. Such effects also enter in the case of quasielastic reactions with (anti)neutrinos and give additional contribution to the vector and axial vector current matrix elements. These are called meson exchange current (MEC) effects. It has also been shown that such effects appear in the vector currents as a necessary consequence of gauge invariance of electromagnetic interactions in the presence of two nucleon potentials. Therefore, the gauge invariant part can be calculated in a model independent way. However, the contribution from the MEC in the axial vector sector and part of the contributions from the vector current are model dependent. The MEC effects are studied quite well in the low energy electroweak processes leading to the quenching of g_1 and the magnetic moment in nuclei; they are also important in quasielastic reactions.

(v) **Short range and long range nucleon–nucleon correlations**

The nucleons in nuclei are highly correlated with the long range correlations arising from pion exchanges as well as the short range correlations due to exchange of ρ and other heavy mesons. In simple models of the Fermi gas type, long range correlations are handled through the random phase approximation (RPA). The long range and short range correlations are taken into account in more sophisticated calculations in a model dependent way in which two-body and three-body nucleon–nucleon potentials are considered along with the central potential to calculate the nucleon wave functions in

https://doi.org/10.1017/9781108489065.015 Published online by Cambridge University Press

the initial and final states. Such calculations are also done in the case of low energy exclusive reactions of nuclei. In the region of high energy inclusive reactions, such multinucleon correlation effects are included in the ground state only in the context of closure approximations.

The nucleon–nucleon correlation effects due to the two particle–two hole ($2p-2h$) excitations calculated using the relativistic Fermi gas model in (anti)neutrino reactions have been recently shown to play a very important role in understanding present day neutrino experiments using nuclear targets (Section 14.7). Such correlation effects are well known in electromagnetic reactions in which pp or np pair is emitted in the electron scattering. It is likely that two such nucleon emission processes will be studied in neutrino reactions using LArTPC detectors in near future; the study of these processes will help to understand the role of short range correlations in $\nu(\bar{\nu})$ reactions from nuclear targets.

It should also be kept in mind that the meson exchange current effects and the nucleon–nucleon correlation effects may influence each other. It is very important to avoid double counting while discussing these effects in theoretical models.

(vi) **Final state interactions and quasielastic like events**

One of the most important nuclear medium effects is due to the final state interactions of hadrons which are produced in the reaction along with leptons. Some of these hadrons would re-scatter giving rise to inelastic reactions but some of them may be re-absorbed by the nucleus, thus mimicking the quasielastic events in which only leptons are produced. These events are called quasielastic-like events. However, such leptons will appear in a different kinematical region and model calculations show that the peak for such events are shifted by almost 150 MeV at $E_\nu = 1$ GeV. The role of such events need to be understood in the case of inclusive quasielastic reactions. Such quasielastic-like events have been a source of major concern since the early neutrino experiments with nuclear targets at CERN [110]. A theoretical understanding of such quasielastic-like events and their role in the present day neutrino oscillation experiments has been shown to be very important.

(vii) **Neutrino energy reconstruction and nuclear medium effects**

(Anti)neutrino experiments on nuclear targets have been done with a continuous beam of (anti)neutrinos having a narrow or wide band neutrino spectrum. Unlike electron beams, (anti)neutrino beams are not monoenergetic. Therefore, studying the energy dependence of (anti)neutrino cross sections is a difficult task. In some of the earlier experiments, the energy of the incident neutrino beam (and therefore, the flux) was determined from the $q^2 \to 0$ limit of the cross section which has very simple energy dependence (see Chapter 10). However, in the case of nuclear targets, even a slight deviation from $q^2 = 0$ corresponding to the spread of the experimental q^2-bin results in the nuclear effects becoming very important; the energy reconstruction also becomes model dependent. In some other experiments, the quasielastic kinematics of lepton production is inverted to obtain the incident neutrino energy in terms of the lepton variables, that is, the energy E' and the scattering angle θ. We get the reconstructed energy E_ν^{rec} and the momentum transfer Q^2_{rec} as:

https://doi.org/10.1017/9781108489065.015 Published online by Cambridge University Press

$$E_\nu^{\rm rec} = \frac{M_p^2 + 2E_\mu M_n - M_n^2 - m_\mu^2}{2(M_n - E_\mu + \cos\theta_\mu)\sqrt{E_\mu^2 - m_\mu^2}}. \tag{14.13}$$

$$Q^2_{\rm rec} = 2E_\nu^{\rm rec}(E_\mu - \cos\theta_\mu\sqrt{E_\mu^2 - m_\mu^2} - m_\mu^2). \tag{14.14}$$

In deriving this result, we have used the relation $p^2 = M_n^2$ and $p'^2 = M_p^2$. However, in the nuclear case, $M_n \to M_n - E_B$, where E_B is the binding energy and $p_n \neq 0$, that is, $p_n^2 = (M_n - E_B)^2 - \vec{p}_n^{\,2}$, where $\vec{p}_n$ has a distribution given by the spectral function. Therefore, in order to reconstruct the neutrino energy, we have to:

i) make some assumptions about the spectral function of the nucleon inside the nucleus,

ii) separate, kinematically, the quasielastic events from the quasielastic-like lepton events which have different kinematics and might overlap with the kinematical region of true quasielastic events due to the momentum distribution of target nucleons in the nucleus.

14.3 General Considerations

The general formulation for studying the quasielastic scattering of (anti)neutrinos from nuclear targets is developed in analogy with the theory of quasielastic electron scattering from nuclei using impulse approximation. In impulse approximation, the nuclear cross section is assumed to be the incoherent sum of the nucleon cross section calculated using single nucleon operators as shown in Figure 14.3.

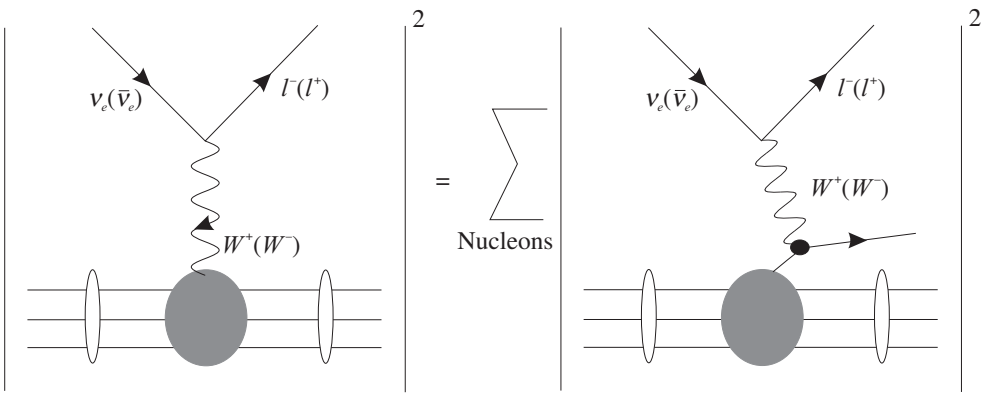

Figure 14.3 Neutrino–nucleus scattering in the impulse approximation in which W interacts with a single nucleon.

It is evident that this description is not sufficient to represent the real physical situation as the effects due to meson exchange currents (MEC) and final states interaction (and also the initial state interaction) as shown in Figure 14.4 shall always be present.

In order to study the corrections to the impulse approximation arising due to these effects, a good understanding of nuclear wave functions of the initial and final states in the presence of

https://doi.org/10.1017/9781108489065.015 Published online by Cambridge University Press

nucleon–nucleon correlations as well as the final state interactions is required. However, in the case of inclusive quasielastic scattering in which only leptons are observed in the final state, a good knowledge of the ground state wavefunction or ground state density would be needed in a closure approximation. Such knowledge of ground state density (and wave function) in several nuclei is available from the experiments done on quasielastic electron scattering from nuclei.

There are various theoretical approaches which have been used to calculate the $\nu(\bar{\nu})$ scattering cross section from the nuclear targets for exclusive reactions which differ from each other in their treatment of nucleons in the nucleus. The exclusive reactions are calculated using microscopic approaches in which a nuclear wavefunction, calculated in a shell model with central potential, incorporates the nucleon–nucleon correlations with a two-body potential through various approaches like the random phase approximation (RPA) [638, 639, 640, 641, 642, 643], continuous random phase approximation (CRPA) [644, 645, 646, 647, 648], quasi particle random phase approximation (QRPA) [649, 650, 651, 652, 653], projected QRPA [654], relativistic RPA [655], and relativistic nuclear energy density functional (RNEDF) [656], etc.

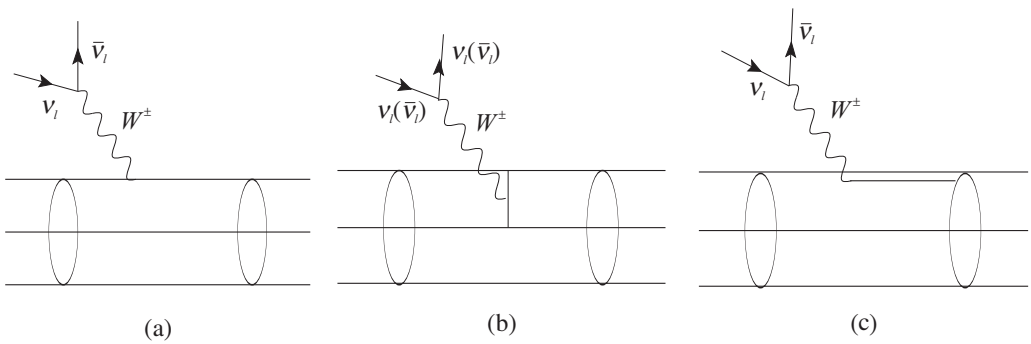

Figure 14.4 Neutrino–nucleus scattering with (a) final state interactions (b) exchange currents due to mesons and (c) exchange currents due to Δ.

In the case of inclusive reactions relevant for intermediate and high energy neutrinos from the accelerator and atmospheric sources, the application of impulse approximation with experimentally determined ground state densities or wave function has given reasonable results in various calculations done in a nuclear structure type calculation or in a Fermi gas model type calculations. However, in the case of exclusive or semi-inclusive reactions a few discrete nuclear states are excited especially in the region of low energy $\nu(\bar{\nu})$ reactions relevant for solar and reactor neutrinos. In such reactions a comprehensive knowledge of the nuclear wavefunction is required whose parameters are determined from theoretical and experimental studies of quasielastic electron nucleus scattering in nuclei like ^{12}C, ^{16}O, etc. In the case of inclusive reactions, various approaches like the nonrelativistic Fermi gas model [294], the relativistic Fermi gas model [657, 658], the local Fermi gas model [659, 660, 661, 662, 663, 664, 665, 666, 667, 668] with and without RPA, the relativistic mean field theory [669, 670, 671, 672, 673], the relativistic Green function with complex optical potential [670, 671, 672, 674] and superscaling approximation(SuSA) [637] have been used.

https://doi.org/10.1017/9781108489065.015 Published online by Cambridge University Press

The theoretical structure of the basic reactions on the nucleon induced by the weak charged (CC) and neutral current(NC) is given by the standard model which has been discussed in Chapter 10. A further simplification occurs in case of nuclei, where nucleons are nonrelativistic and the nonrelativistic limit of the transition operators can be used as given in Appendix A. As discussed in Chapter 10, the strength of various form factors and their q^2 dependence may change in the presence of a nuclear medium subjected to the symmetry properties of the weak current in the CC and NC sectors but our approach is to take their values for the case of free nucleons and examine the effect of the nuclear medium on them.

In the following, we outline the basic ingredients needed to calculate the exclusive and inclusive reactions utilizing the simplest models to illustrate the methods used at low and intermediate energies.

14.4 Low Energy Quasielastic Reactions

14.4.1 Multipole expansion of the matrix elements

The low energy quasielastic reaction leads to the ground state or the excited states of the final nucleus. If the initial and final nuclear states are denoted by $|i\rangle$ and $|f\rangle$, then the transition matrix element $\mathcal{M}_{fi}$ is defined as

$$\begin{aligned} \mathcal{M}_{fi} &= \langle f|\mathcal{H}|i\rangle, \\ \text{where} \quad \mathcal{H} &= -\frac{G_F\cos\theta_C}{\sqrt{2}}\int d\vec{x}\, l^\mu\, J_\mu(x). \end{aligned} \tag{14.15}$$

Here, l^μ is the leptonic current and J_μ is the hadronic current operator in the nucleus. Since the leptons in Eq. (14.4) are point particles, we can describe them by plane waves (neglecting the Coulomb distribution of the charged lepton in the final state), to write

$$l_\mu(x) = l_\mu e^{-i\vec{q}\cdot\vec{x}}, \qquad q = k' - k = p - p', \tag{14.16}$$

such that the matrix element $\mathcal{M}_{fi}$ between the initial and final states $|i\rangle$ and $|f\rangle$ is written as

$$\begin{aligned} \mathcal{M}_{fi} &= -\frac{G_F\cos\theta_C}{\sqrt{2}}\langle f|\int e^{-iq\cdot x} l^\mu J_\mu(x) d\vec{x}|i\rangle \\ &= -\frac{G_F\cos\theta_C}{\sqrt{2}}\langle f|\int e^{-iq\cdot x}(l^0 J_0 - \vec{l}\cdot\vec{J}) d\vec{x}|i\rangle. \end{aligned} \tag{14.17}$$

To make a multipole expansion of the matrix element [675, 676] in Eq.(14.17), we express the scalar product $\vec{l}\cdot\vec{J}e^{-iq\cdot x}$ using $\vec{l}$ in spherical basis by writing

$$\vec{l} = \sum_\lambda l_\lambda \hat{e}^\dagger_\lambda, \tag{14.18}$$

where $\hat{e}_\lambda(\lambda = \pm 1, 0)$ are the components of the unit vector $(\hat{e}_x, \hat{e}_y, \hat{e}_z)$ in the spherical basis defined as

$$e_{\pm 1} = \pm\frac{\hat{e}_x \pm i\hat{e}_y}{\sqrt{2}}, \qquad \hat{e}_0 = \hat{e}_z, \tag{14.19}$$

https://doi.org/10.1017/9781108489065.015 Published online by Cambridge University Press

satisfying $\vec{e}_\lambda \cdot \vec{e}_{\lambda'} = \delta_{\lambda\lambda'}$, such that $l_\lambda = \vec{l} \cdot \hat{e}_\lambda$.

We use the multipole expansion for $e^{i\vec{q}\cdot\vec{x}}$, that is,

$$e^{i\vec{q}\cdot\vec{x}} = \sum_{l=0}^{\infty} \sqrt{4\pi(2l+1)}\; i^l j_l(qx) Y_{l0}(\Omega_x), \tag{14.20}$$

where $q = |\vec{q}|$ and $Y_{l0}(\Omega_x)$ are the spherical harmonics and $j_J(qx)$ are the spherical Bessel's function.

The vector spherical harmonics $\vec{\mathcal{Y}}^M_{Jl1}$ are defined as

$$\vec{\mathcal{Y}}^M_{Jl1} = \sum_{m\lambda} \langle lm1\lambda | l1JM\rangle Y_{lm}(\theta,\phi)\vec{e}_\lambda, \tag{14.21}$$

where $\langle lm1|\lambda|l1JM\rangle$ are the Clebsch–Gordan (CG) coefficients.

Using the definition of the vector spherical harmonics given in Eq. (14.21) and choosing $\hat{q} \parallel \hat{e}_z$, that is, the unit vector along the Z-axis with the orthogonality property of CG coefficients, we write

$$\vec{e}_\lambda e^{i\vec{q}\cdot\vec{x}} = \sum_l \sum_{J=0}^{\infty} \sqrt{4\pi(2l+1)}\; i^J j_l(q,x) \langle l01\lambda | l1J\lambda\rangle \vec{\mathcal{Y}}^\lambda_{JL1}, \quad x = |\vec{x}|. \tag{14.22}$$

In Eq. (14.22), we perform the expansion over l, using the values of the CG coefficients for $\lambda = \pm 1$ and $\lambda = 0$ explicitly. There would be, in general, three terms for each $\lambda(= \pm 1, 0)$, corresponding to $l = J+1, J, J-1$. Using the nonvanishing values of the CG coefficients in each case, the following properties of the vector spherical harmonics, that is, [676]

$$\vec{\nabla}_r \times j_J(r)\vec{\mathcal{Y}}^M_{JJ1} = -i\Big(\frac{J}{2J+1}\Big)^{\frac{1}{2}} j_{J+1}(r)\vec{\mathcal{Y}}^M_{J,J+1,1} + i\Big(\frac{J+1}{2J+1}\Big)^{\frac{1}{2}} j_{J-1}(r)\vec{\mathcal{Y}}^M_{J,J-1,1}, \tag{14.23}$$

$$\vec{\nabla} r j_J(r) Y_{JM} = \Big(\frac{J+1}{2J+1}\Big)^{\frac{1}{2}} j_{J+1}(r)\vec{\mathcal{Y}}^M_{J,J+1,1}\Big(\frac{J}{2J+1}\Big)^{\frac{1}{2}} j_{J-1}(r)\vec{\mathcal{Y}}^M_{J,J-1,1}, \tag{14.24}$$

the expression for $\vec{e}_\lambda e^{i\vec{q}\cdot\vec{x}}$ given in Eq. (14.22) is evaluated.

After performing some basic algebraic manipulations, the following expressions are obtained:

$$\begin{aligned}
\vec{e}_{\vec{q}\lambda} e^{i\vec{q}\cdot\vec{x}} &= -\frac{i}{q}\sum_{J=0}^{\infty}[4\pi(2J+1)]^{\frac{1}{2}} i^J \vec{\nabla}(j_J(qx)Y_{J0}(\Omega_x)), \quad \text{for } \lambda = 0 \\
&= -\sum_{J\geq 1}^{\infty}[2\pi(2J+1)]^{\frac{1}{2}} i^J \Big[\lambda_{j_J}(qx)\vec{\mathcal{Y}}^\lambda_{JJ1} \\
&\quad + \frac{1}{q}\vec{\nabla}\times(j_J(qx))\vec{\mathcal{Y}}^\lambda_{JJ1}\Big], \quad \text{for } \lambda = \pm 1.
\end{aligned} \tag{14.25}$$

Therefore, the matrix element in Eq. (14.17) is written as

$$\langle f|\mathcal{H}|i\rangle = -\frac{G}{\sqrt{2}}\langle f|\Big(-\sum_{\lambda=\pm1} l_\lambda \sum_{J\geq 1}^{\infty}[2\pi(2J+1)]^{\frac{1}{2}}(-i)^J$$

https://doi.org/10.1017/9781108489065.015 Published online by Cambridge University Press

$$\times[\lambda\hat{T}^{\rm mag}_{J-\lambda}(q)+\hat{T}^{el}_{J-\lambda}(q)]$$
$$+\sum_{J=0}^{\infty}[4\pi(2J+1)]^{\frac{1}{2}}(-i)^J[l_3\hat{L}_{J0}(q)-l_0\hat{C}_{J0}(q)]\Big)|i\rangle, \tag{14.26}$$

where

$$\hat{C}_{JM}(q) \equiv \hat{C}^V_{JM}+\hat{C}^A_{JM}\equiv\int d\vec{x}[j_J(qx)Y_{JM}(\Omega_x)]J_0(\vec{x}), \tag{14.27}$$

$$\hat{L}_{JM}(q) \equiv \hat{L}^V_{JM}+\hat{L}^A_{JM}\equiv\frac{i}{q}\int d\vec{x}[\vec{\nabla}(j_J(qx)Y_{JM}(\Omega_x))]\cdot\vec{J}(\vec{x}), \tag{14.28}$$

$$\hat{T}^{el}_{JM}(q) \equiv \hat{T}^{V,el}_{JM}+\hat{T}^{A,el}_{JM}\equiv\frac{i}{q}\int d\vec{x}[\vec{\nabla}_\times j_J(qx)\vec{\mathcal{Y}}^M_{JJ1}]\cdot\vec{J}(\vec{x}), \tag{14.29}$$

$$\hat{T}^{\rm mag}_{JM}(q) \equiv \hat{T}^{V,{\rm mag}}_{JM}+\hat{T}^{A,{\rm mag}}_{JM}\equiv\int d\vec{x}[j_J(qx)\vec{\mathcal{Y}}^M_{JJ1}]\cdot\vec{J}(\vec{x}). \tag{14.30}$$

Here, C_{JM}, L_{JM}, T^{el}_{JM} and $T^{\rm mag}_{JM}$ are called multipoles.

In the following, we enumerate some features of the aforementioned multipoles

(i) The $C_{JM}(q), L_{JM}(q), T^{el}_{JM}(q)$, and $T^{\rm mag}_{JM}(q)$ are called, respectively, the Coulomb, longitudinal, transverse electric, and transverse magnetic multipoles.

(ii) The angular momentum sum in the expression for Coulomb and longitudinal multipoles starts from $J=0$ as they depend upon the spherical harmonics $Y_{JM}(\Omega)$; while the transverse multipole starts from $J=1$ as they depend upon the vector spherical harmonics $\vec{y}_{JJ1}(\Omega)$.

(iii) Since the weak current operator J^μ appearing in the definition of multipoles contains vector and axial vector currents, that is, $J^\mu=V^\mu+A^\mu$, the multipoles are classified as vector and axial vector multipoles and are written as:

$$M_{JM}\Rightarrow M^V_{JM}(q)+M^A_{JM}(q)$$

for each $M_{JM}=C_{JM}, L_{JM}, T^{el}_{JM}, T^{\rm mag}_{JM}$, where $M^V_{JM}(q)$ and $M^A_{JM}(q)$ are the multipoles corresponding to vector and axial vector currents.

(iv) The parity of the vector and axial vector multipoles $M^V_{JM}(q)$ and $M^A_{JM}(q)$ are opposite to each other. The parity of M^V_{JM} is defined in the conventional way with reference to the electromagnetic vector current. The parity of all the vector and axial vector multipoles are shown in Table 14.1.

Table 14.1 Parity of vector and axial vector multipoles.

Multipole	C^V_{JM}	L^V_{JM}	$T^{el,V}_{JM}$	$T^{\rm mag,V}_{JM}$	C^A_{JM}	L^A_{JM}	$T^{el,A}_{JM}$	$T^{\rm mag,A}_{JM}$
Parity	$(-1)^J$	$(-1)^J$	$(-1)^J$	$(-1)^{J+1}$	$(-1)^{J+1}$	$(-1)^{J+1}$	$(-1)^{J+1}$	$(-1)^J$

https://doi.org/10.1017/9781108489065.015 Published online by Cambridge University Press

(v) In general, there are eight multipoles to be considered, four corresponding to vector currents and four corresponding to the axial vector currents. However, since the vector current is conserved,

$$q_\mu J^\mu = 0 \tag{14.31}$$

implying

$$q_0 J^0 = \vec{q} \cdot \vec{J}. \tag{14.32}$$

Taking $\vec{q} \parallel \hat{e}_z$, we get a relation between the Coulomb and longitudinal multipoles, that is,

$$q_0 \langle J_f | C^V_{JM} | J_i \rangle - \vec{q} \langle J_f | L^V_{JM} | J_i \rangle = 0. \tag{14.33}$$

Therefore, the $\nu(\bar{\nu})$ cross sections are given in terms of seven multipoles while the electron scattering is described in terms of three multipoles.

(vi) The single nucleon current operators J^μ to be used with the nuclear wave functions in the impulse approximation are derived from the definition of the matrix elements of the vector and axial vector currents between free nucleon states given in Chapter 10. In the case of a nucleus, the nucleons are treated nonrelativistically; therefore, the nonrelativistic reduction of the current operators given in Appendix A can be used. We obtain for J^μ in the lowest order of momenta, neglecting the term $O(\frac{\vec{q}^2}{M^2})$, $O(\frac{\vec{p}^2}{M^2})$, and writing J^μ as

$$J^\mu = (J^0, \vec{J}), \tag{14.34}$$

where

$$J^0 = \left(f_1(q^2) + g_1(q^2) \vec{\sigma} \cdot \frac{2\vec{p} - \vec{q}}{2M} \right) \tau^\pm \tag{14.35}$$

$$\vec{J} = \left(g_1(q^2) \vec{\sigma} - i(f_1(q^2) + 2M f_2(q^2)) \frac{\vec{\sigma} \times \vec{q}}{2M} \right) \tau^\pm + f_1(q^2) \frac{2\vec{p} - \vec{q}}{2M} \tau^\pm. \tag{14.36}$$

It should be noted that the terms involving $\frac{q_0}{2M}$ are of the order of $O(\frac{q^2}{4M^2})$ because $q_0 = -\frac{q^2}{2M}$ for elastic scattering and are, therefore, neglected in the case of nuclear transitions at low energies. The operator $\tau^{+(-)}$ corresponds to the $\nu(\bar{\nu})$ scattering processes. The nuclear operators corresponding to the nucleon operators given in Eqs. (14.35) and (14.36) are therefore given by:

$$J^0(x) = \sum_{i=1}^{A} \left[f_1(q^2) \delta(\vec{x} - \vec{x}_i) + g_1(q^2) \left(\frac{p(i)}{M} \delta(\vec{x} - \vec{x}_i) \right)_{\text{sym}} \right] \tau^\pm, \tag{14.37}$$

https://doi.org/10.1017/9781108489065.015 Published online by Cambridge University Press

$$\vec{J}(x) = \sum_{i=1}^{A}\left[g_1(q^2)\vec{\sigma} + f_1(q^2)\frac{2\vec{p}\cdot\vec{q}}{2M} - i\frac{f_1(q^2)+2M(q^2)}{2M}\vec{\sigma}(i)\times\vec{q}\right]\delta(\vec{x}-\vec{x}_i)\tau^{\pm}, \tag{14.38}$$

where $\vec{x}_i$ is the position coordinate of the ith interacting nucleon. This shows that there are various operators in the nuclear space which enter in the current $J^0(x)$ and $\vec{J}(x)$, for the multipoles which are of the type $\tau^{\pm}(i)$, $\tau^{\pm}(i)\sigma(i)$, and $\tau^{\pm}(i)\vec{p}(i)(=-i\tau^{\pm}(i)\vec{\nabla}(i))$ multiplied by the spherical harmonics, vector spherical harmonics, and the gradient and curl operators of the vector spherical harmonics as shown in the definition of the multipoles in Eqs. (14.27)–(14.30).

14.4.2 Cross sections

The cross sections for the quasielastic scattering from nuclei using the non-relativistic kinematics for nucleons is written as:

$$\frac{d\sigma}{d\Omega} = \frac{k'E'}{(2\pi)^2}\sum_{\text{lepton spins}}\overline{\sum}_{\text{nucleon spins}}|\langle f|\mathcal{H}|i\rangle|^2. \tag{14.39}$$

If the initial ($|i\rangle$) and final states ($|f\rangle$) are specified by the angular momentum states $|J_iM_i\rangle$ and $|J_fM_f\rangle$, respectively, then

$$\frac{d\sigma}{d\Omega} = \frac{k'E'}{(2\pi)^2}\sum_{\text{lepton spins}}\frac{1}{2J_l+1}\sum_{M_i}\sum_{M_f}\left|\langle J_fM_f|\mathcal{H}|J_iM_i\rangle\right|^2. \tag{14.40}$$

Since the operators in H_W transform as definite multipoles $M_{JM}(M_{JM} = C_{JM}, L_{JM}, T^{el}_{JM}, T^{\text{mag}}_{JM})$ with specified values of J and M, we use the Wigner–Eckart theorem to write

$$\langle J_fM_f|M_{JM}|J_iM_i\rangle = (-1)^{J_f-M_f}\begin{pmatrix} J_f & J & J_i \\ -M_f & M & M_i\end{pmatrix}\langle J_f||M_J||J_i\rangle. \tag{14.41}$$

For an unpolarized nucleon target and no observation made on the final nucleon, we sum over all the M_f states and average over M_i states to obtain

$$\frac{1}{2J_i+1}\sum_{M_i}\sum_{M_f}\begin{pmatrix} J_f & J & J_i \\ -M_f & M & M_i\end{pmatrix}\begin{pmatrix} J_f & J' & J_i \\ -M_f & M' & M_i\end{pmatrix} = \delta_{JJ'}\delta_{MM'}\frac{1}{2J+1}\frac{1}{2J_i+1}. \tag{14.42}$$

We use this relation and the identity that

$$\sum_{\lambda=\pm1} l_\lambda l^*_\lambda(a+\lambda b)^2 = (l\cdot l^* - l_3l^*_3)(|a|^2+|b|^2) - 2i(\vec{l}\times\vec{l}^*)_3\text{Re}(a^*b), \tag{14.43}$$

https://doi.org/10.1017/9781108489065.015 Published online by Cambridge University Press

The following result is obtained [676],

$$\begin{aligned}\frac{1}{2J_i+1}\sum_{M_i}\sum_{M_f}|\langle f|\hat{H}_W|i\rangle|^2 &= \frac{G^2}{2}\frac{4\pi}{2J_i+1}\Big[\sum_{J\geq 1}^{\infty}\Big(\frac{1}{2}(\vec{l}\cdot\vec{l}^{\,*}-l_3l_3^*)(|\langle J_f||\hat{T}_J^{\rm mag}||J_i\rangle|^2 \\ &\quad +|\langle J_f||\hat{T}_J^{el}||J_i\rangle|^2) \\ &\quad -\frac{i}{2}(\vec{l}\times\vec{l}^{\,*})_3\,2{\rm Re}\langle J_f||\hat{T}_J^{\rm mag}||J_i\rangle\langle J_f||\hat{T}_J^{el}||J_i\rangle^*\Big) \\ &\quad +\sum_{J=0}^{\infty}\Big(l_3l_3^*|\langle J_f||\hat{L}_J||J_i\rangle|^2+l_0l_0^*|\langle J_i||\hat{M}_J||J_i\rangle^*|^2 \\ &\quad -2{\rm Re}l_3l_3^*\langle J_f||\hat{L}||J_i\rangle\langle||\hat{M}_J||J_i\rangle^*\Big)\Big]. \end{aligned} \tag{14.44}$$

Further, using the leptonic tensor $\sum_{spin} l_\mu l_\nu = \delta(k_\mu k'_\nu + k_\nu k'_\mu - g_\mu\nu k\cdot k' + i\epsilon_{\mu\nu\rho\sigma}k^\rho k^\sigma)$, we obtain the following result for the quasielastic nuclear cross sections

$$\begin{aligned}\left(\frac{d\sigma}{d\Omega}\right)_{\nu\bar{\nu}} &= \left(\frac{q}{\epsilon}\right)\frac{G^2\epsilon^2}{4\pi^2}\frac{4\pi}{2J_i+1}\Big[\Big[\sum_{J=0}^{\infty}\{(1+\hat{v}\cdot\vec{\beta})|\langle J_f||\hat{M}_J||J_i\rangle|^2 \\ &+ [1-\hat{v}\cdot\vec{\beta}+2(\hat{v}\cdot\vec{\beta})(\hat{q}\cdot\vec{\beta})]|\langle J_f||\hat{L}_J||J_i\rangle|^2 \\ &- [\hat{q}\cdot(\hat{v}+\vec{\beta})]\,2\,{\rm Re}\langle J_f||\hat{L}_J||J_i\rangle\langle J_f||\hat{M}_J||J_i\rangle^*\} \\ &+ \sum_{J\geq 1}^{\infty}\{[1-(\hat{v}\cdot\hat{q})(\hat{q}\cdot\vec{\beta})][|\langle J_f||\hat{T}_J^{\rm mag}||J_i\rangle|^2+|\langle J_f||\hat{T}_J^{el}||J_i|^2] \\ &\pm [\hat{q}\cdot(\hat{v}-\vec{\beta})]\,2\,{\rm Re}\langle J_f||\hat{T}_J^{\rm mag}||J_i\rangle\langle J_f||\hat{T}_J^{el}||J_i\rangle^*\}\Big]\Big], \end{aligned} \tag{14.45}$$

where $\hat{v}\equiv\dfrac{\vec{v}}{|\vec{v}|}$, $\hat{q}\equiv\dfrac{\vec{q}}{|\vec{q}|}$.

Since the ν_e $(\bar{\nu}_e)$ used in the calculations with reactor and solar neutrinos are in the range of a few MeV, the electrons produced in these reactions can be treated relativistically. Similarly, in the case of (anti)neutrino reactions induced by the ν_μ $(\bar{\nu}_\mu)$ of energies in the range of a few hundreds of MeV and GeV, the muons in the final state can also be treated relativistically. Therefore, in most calculations, Eq. (14.45) is used in the relativistic limit. In this limit, it is given by:

$$\begin{aligned}\left(\frac{d\sigma}{d\Omega}\right)^{RL}_{\nu\bar{\nu}} &= \frac{G^2\epsilon^2}{2\pi^2}\frac{4\pi}{2J_i+1}\left[\cos^2\frac{\theta_C}{2}\left(\sum_{J=0}^{\infty}|\left\langle J_f\left|\left|\hat{M}_J-\frac{q^0}{\vec{q}}\hat{L}_J\right|\right|J_i\right\rangle|^2\right)\right. \\ &+ \left(\frac{q^2}{2|\vec{q}|^2}\cos^2\frac{\theta}{2}+\sin^2\frac{\theta}{2}\right)\left(\sum_{J\geq 1}^{\infty}\left(|\langle J_f||\hat{T}_J^{\rm mag}||J_i\rangle|^2+|\langle J_f||\hat{T}_J^{el}||J_i\rangle|^2\right)\right) \\ &\mp \sin\frac{\theta}{2}\frac{1}{|\vec{q}|}\left(q^2\cos^2\frac{\theta}{2}+|\vec{q}|^2\sin^2\frac{\theta}{2}\right)^{1/2} \\ &\quad \left.\left(2\,{\rm Re}\langle J_f||\hat{T}_J^{\rm mag}||J_i\rangle\langle J_f||\hat{T}_J^{el}||J_i\rangle^*\}\right)\right]. \end{aligned} \tag{14.46}$$

https://doi.org/10.1017/9781108489065.015 Published online by Cambridge University Press

This is the general result which is used to calculate the nuclear cross section for quasielastic ν and $\bar{\nu}$ reactions leading to discrete nuclear states. Once the initial and final states are fixed, only the multipoles which are compatible with change in the angular momentum and parity would contribute.

14.4.3 Single particle matrix element in the shell model of nuclei

The single particle wave functions in the shell model are characterized by the quantum numbers $n, l, s(=\frac{1}{2}), J$, and M, where the orbital angular momentum l is coupled to the spin s to give the total angular momentum J with $J_Z(=M)$ as the third component of the total angular momentum. The initial and final states $|i\rangle$ and $|f\rangle$ are, therefore, written as:

$$|i\rangle = |n(l\frac{1}{2})J_i M_i\rangle. \tag{14.47}$$

$$|f\rangle = |n(l'\frac{1}{2})J_f M_f\rangle. \tag{14.48}$$

where

$$|n(l\frac{1}{2})|JM\rangle = \psi_{nl\frac{1}{2}JM}(r) = NR_{nl}[Y_{lm}(\theta,\phi)\otimes\psi_{\frac{1}{2}m_j}]_{JM}\,. \tag{14.49}$$

Here, $R_{nl}(r)$ is a radial wave function of the nucleus obtained as a solution of nucleons moving in a potential, say a simple harmonic oscillator potential or any other potential which includes the effect of correlation in addition to a central potential.

The reduced matrix element of the multipoles are expressed as:

$$\langle n'(l'\frac{1}{2}J_f)||M_{JM}||n(l\frac{1}{2}J_i)\rangle \tag{14.50}$$

for various $M_{JM}^{V(A)}(M_{JM} = C_{JM}^{V(A)}, L_{JM}^{V(A)}, T_{JM}^{el\ V(A)}, T_{JM}^{mag\ V(A)})$ in case of vector and axial vector multipoles. The aforementioned reduced matrix elements are calculated using the expression for the weak current operator J^μ for the free nucleons given in Eq. (14.34) and the expressions in the coordinate space in the case of nuclei as given in Eqs. (14.37) and (14.38) in terms of the operators $\tau^{\pm}(i), \tau^{\pm}(i)\vec{\sigma}(i)$, and $-i\tau^{\pm}(i)\vec{\nabla}(i)$. The multipole operators M_{JM}, are then expressed in terms of the various nuclear operators. Introducing the notation

$$M_J^M(\vec{x}) = j_J(qx)Y_{JM}(\Omega_x), \tag{14.51}$$

$$\vec{M}_{JL}^M(\vec{x}) = j_L(qx)\vec{\mathcal{Y}}_{JL1}^M(\Omega_x), \tag{14.52}$$

and using some complicated algebraic manipulations, the various multipole operators are derived as [676]

$$M_{JM} = f_1 M_J^M(\vec{x}_i), \tag{14.53}$$

$$L_{JM} = \frac{q_0}{|\vec{q}|} f_1 M_J^M(\vec{x}_i), \tag{14.54}$$

https://doi.org/10.1017/9781108489065.015 Published online by Cambridge University Press

$$T^{el}_{JM} = \frac{f_1}{M_n}\Big[-\Big(\frac{J}{2J+1}\Big)^{\frac{1}{2}}\vec{M}^M_{J,J+1}(\vec{x}_i) + \Big(\frac{J+1}{2J+1}\Big)^{\frac{1}{2}}\vec{M}^M_{J,J-1}(x_i)\Big]\cdot\vec{\nabla}(i) + \frac{|\vec{q}|}{2M_n}(f_1+2M_nf_2)\vec{M}^M_{JJ}(\vec{x})\cdot\vec{\sigma}(i), \quad (14.55)$$

$$T^{\text{mag}}_{JM} = \frac{f_1}{iM_n}\vec{M}^M_{JJ}(\vec{x}_i)\cdot\vec{\nabla}(i) + \frac{|\vec{q}|}{2M_n}(f_1+2M_nf_2)\times\Big[-i\Big(\frac{J}{2J+1}\Big)^{\frac{1}{2}}\vec{M}^M_{J,J+1}(\vec{x}_i) + i\Big(\frac{J+1}{2J+1}\Big)^{\frac{1}{2}}\times\vec{M}^M_{J,J-1}(\vec{x}_i)\Big]\cdot\vec{\sigma}(i), \quad (14.56)$$

$$T^{mag,A}_{JM} = g_1\vec{M}^M_{JJ}(\vec{x}_i)\cdot\vec{\sigma}(i), \quad (14.57)$$

$$T^{el,A}_{JM} = g_1\Big[-i\Big(\frac{J}{2J+1}\Big)^{\frac{1}{2}}\vec{M}^M_{J,J+1}(\vec{x}_i) + i\Big(\frac{J+1}{2J+1}\Big)^{\frac{1}{2}}\vec{M}^M_{J,J-1}(\vec{x}_i)\Big]\cdot\vec{\sigma}(i), \quad (14.58)$$

$$M^A_{JM} = \frac{g_1}{iM_n}M^M_J(\vec{x}_i)[\vec{\sigma}(i)\cdot\vec{\nabla}(i)] - \frac{|\vec{q}|}{2M_ng_1}g_1L^A_{JM}, \quad (14.59)$$

$$\text{where, } L^A_{JM} \equiv g_1\Big[i\Big(\frac{J+1}{2J+1}\Big)^{\frac{1}{2}}\vec{M}^M_{J,J+1}(\vec{x}_i) + i\Big(\frac{J}{2J+1}\Big)^{\frac{1}{2}}\vec{M}^M_{J,J-1}(\vec{x}_i)\Big]\cdot\vec{\sigma}(i). \quad (14.60)$$

We see that all the multipoles can be evaluated using the matrix element of the operator $M_J(x_i)$, $\vec{M}_{Jl}(x_i).\vec{\nabla}(x_i)$, and $\vec{M}_J(x_i).\vec{\sigma}(i)$ taken between the states $|n(\frac{1}{2})J_fM_f\rangle$ and $|n(\frac{1}{2})J_iM_i\rangle$. The explicit expressions for these matrix elements are available in literature. Recently, Haxton and Lunardini [677] have provided a software in Mathematica to evaluate the algebraic expressions and the integrals needed to calculate these matrix elements and the cross sections in Eq. (14.46).

14.5 Quasielastic $\nu(\bar{\nu})$ Reactions at Intermediate Energies

14.5.1 Introduction

As the energy of neutrinos and antineutrinos increases, there are more nuclear states which are excited. In order to calculate the inclusive quasielastic reaction cross section, one needs to calculate the cross section of all the excited states accessible in the reaction process and sum over them. In most cases, while the ground state of the final nucleus is known reasonably well, the description of the excited states is not adequate. In many cases, while the parameters of the ground state wave functions are also determined experimentally, there is not much information about the excited states. Therefore, the microscopic calculations of the $\nu(\bar{\nu})$ scattering cross section using nuclear wave functions to calculate transitions to excited states are model dependent and suffer from large uncertainties.

The experimental studies of $\nu(\bar{\nu})$ induced reaction cross sections in nuclear targets have been made with reasonable precision in recent years with reference to the analysis of various neutrino oscillation experiments. Most of these experiments involve $\nu(\bar{\nu})$ energies in the range of 500 MeV $< E_{\nu(\bar{\nu})} <$ 2 GeV with maximum flux $\nu(\bar{\nu})$ around 1 GeV. In this energy region and specially around 1 GeV, the quasielastic reactions make a dominant contribution

https://doi.org/10.1017/9781108489065.015 Published online by Cambridge University Press

to the cross sections and the microscopic calculations based on the summation method using multipole expansion described in the earlier section are not adequate. The subject has been reviewed by many authors in recent years [356, 447, 427, 426, 678, 679].

The simplest nuclear model to study (anti)neutrino reactions was the Fermi gas model. In this model, the free nucleon cross section $\frac{d\sigma}{dq^2}$ is multiplied by a factor $(1 - D/N)$, where N is the number of nucleon targets and D is a factor depending upon the four-momentum transfer squared q^2, N, Z, and the Fermi momentum k_F of the target nucleus [633, 635, 294, 680]. This model is extended to the higher energies, that is, the relativistic Fermi gas model (RFG), in which nucleons are treated relativistically and free [657, 658]. The nuclear effects are treated by taking into account the binding energy and the Pauli principle. Recently, the RFG model has been extended to treat the long range nucleon–nucleon correlations within Random phase approximation (RPA) and the initial state interactions by including the nucleon spectral functions, calculated with inputs from experimental information on electron nucleus scattering [356, 447, 426].

Another model which has been used is the shell model with closure approximation in which the initial state is treated in the shell model using a nuclear potential and the contributions from the higher states is summed over all the final states using closure approximation, assuming completeness of states. For this, an average excitation energy is assumed which is treated as a parameter. Since all the final state contributions are summed over, this method is expected to reproduce only the total cross section and its energy dependence.

In view of the importance of the nucleon–nucleon correlation in the initial and final states as well as the final state interactions, the relativistic mean field model (RMF) which is based on the solution of the Dirac equation in the presence of strong scalar and vector potentials, due to the mediating meson fields, has also been used [669, 670, 671, 672, 673]. Similarly, the relativistic Green function models, based on the use of a complex optical potential for nucleon–nucleus interaction to treat the final state interactions, have been used in the context of RMF as well as the conventional shell model approaches [670, 671, 672, 674].

In recent developments, the phenomenological approach based on the superscaling (SuSA) model of electron scattering has been applied to calculate the quasielastic $\nu(\bar{\nu})$ cross sections from nuclear targets [637]. In this approach, which is similar to the Bjorken scaling approach in DIS discussed in Chapter 13, the cross sections are assumed to scale and depend only upon scaling function $F(\xi)$ which is a function of only one variable ξ instead of $|\vec{q}|$ and ω, the momentum and energy transfer. This is a good approximation in the kinematical region, where $|\vec{q}|$ and ω are transferred to a single nucleon which is treated as a free particle in the nucleus and two-body correlations or meson exchange current effects are not significant. As demonstrated in the case of electron scattering, this approximation is appropriate for momentum transfers $|\vec{q}| \geq 400$ MeV/c.

It is not possible to describe all the aforementioned models, so in the following section, we describe only the simplest model, that is, the Fermi gas model and the recent developments using this model to describe quasielastic $\nu(\bar{\nu})$ scattering in nuclei.

https://doi.org/10.1017/9781108489065.015 Published online by Cambridge University Press

14.5.2 Fermi gas model

Nucleons are fermions having spin $\frac{1}{2}$. Therefore, the behavior of the neutron or the proton gas is determined by Fermi–Dirac statistics.

The assumptions of the Fermi gas model are as follows:

- This model considers the nucleus as a degenerate gas of protons and neutrons much like the free electron gas in metals. Nucleons are moving freely inside a nuclear volume (Figure 14.5).
- In such a gas at $T = 0$ K (nucleus in its ground state), all the energy levels up to a maximum, known as Fermi energy E_F, are occupied by particles. In other words, at temperature $T = 0$ K, the lowest states are filled up to a maximum momentum, called the Fermi momentum p_F.

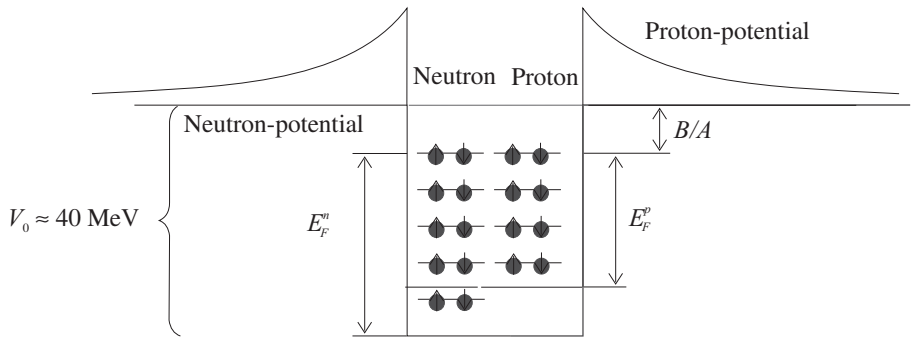

Figure 14.5 Nucleons in a square well potential states.

- Each level is occupied by two identical particles with opposite spins. Protons and neutrons are viewed as two independent systems of nucleons. Two different potential wells for protons and neutrons are considered.
- The average potential that every nucleon feels is a superposition of the potentials due to the other nucleons.
- The neutron potential well is deeper than the proton well because of the missing Coulomb repulsion. The model assumes common Fermi energy for protons and neutrons in stable nuclei; otherwise, $p \rightarrow n$ decay would happen spontaneously. This implies that there are more neutron states available and therefore, $N > Z$ for heavier nuclei.

The simplest version of the Fermi gas model, it was first applied to $\nu(\bar{\nu})$ by Berman [632], following the early work of Gatto [681] and others [294] and gives a suppression factor for the cross section as compared to the free nucleon. It should be mentioned that in these calculations, the suppression factor has a geometric origin derived from the different Fermi spheres for initial and final nucleons in the nucleus and does not depend upon the specific process of scattering.

https://doi.org/10.1017/9781108489065.015 Published online by Cambridge University Press

In case of neutrino scattering on neutrons, the free neutron cross section (Eq. 14.9) is multiplied by a reduction factor $R(q)$, given by

$$\begin{aligned} R_N(q^2) &= 1 - \frac{D(q^2)}{N}, \text{with } D(q^2) = Z \text{ for } \chi < u - v \\ &= \frac{A}{2}\left(1 - \frac{3}{4}\chi\left[u^2 + v^2\right] + \frac{1}{2}\chi^3 - \frac{3}{32\chi}\left[u^2 - v^2\right]^2\right) \text{ for } u - v < \chi < u + v \\ &= 0 \text{ for } \chi > u + v, \end{aligned} \tag{14.61}$$

where $\chi = \frac{|\vec{q}|}{k_F}$, $u = \left(\frac{2N}{A}\right)^{\frac{1}{3}}$, and $v = \left(\frac{2Z}{A}\right)^{\frac{1}{3}}$. N, Z, and A are respectively the neutron, proton, and nucleon numbers and $\vec{q}$ is the three-momentum transfer.

This nonrelativistic global Fermi gas model was later elaborated by Loveseth [635], Yao and others [680] and was extended to relativistic nucleons by Smith and Moniz [657], Gaisser and O'Connell [658]; it is used in some of neutrino event generators for analyzing neutrino oscillation experiments.

In the Fermi gas model, it is assumed that the nucleons in a nucleus (or nuclear matter) occupy one nucleon per unit cell in phase space so that the total number of nucleons N is given by

$$N = 2V \int_0^{p_F} \frac{d\vec{p}}{(2\pi)^3},$$

where a factor of two is added to account for spin degree of freedom. All states up to a maximum momentum p_F ($p < p_F$) are filled. The momentum states higher than $\vec{p} > \vec{p}_F$ are unoccupied.

The occupation number $n(\vec{p})$ is defined as:

$$\begin{aligned} n(\vec{p}) &= 1, \vec{p} < \vec{p}_F \\ &= 0, \vec{p} > \vec{p}_F \end{aligned} \tag{14.62}$$

$$\begin{aligned} \Rightarrow \rho &= \frac{N}{V} = \frac{p_F^3}{3\pi^2}; \\ \text{therefore, } p_F &= \left(\frac{3}{2}\pi^2\rho\right)^{\frac{1}{3}}. \end{aligned} \tag{14.63}$$

Since the protons and neutrons are supposed to have different Fermi sphere,

$$\begin{aligned} p_{F_p} &= \left(3\pi^2\rho_p\right)^{\frac{1}{3}}. \\ p_{F_n} &= \left(3\pi^2\rho_n\right)^{\frac{1}{3}}. \end{aligned} \tag{14.64}$$

The representative values of the Fermi momentum are $p_F = 221$ MeV for carbon, $p_F = 251$ MeV for iron, etc.

Under a weak interaction induced by (anti)neutrinos, a nucleon is excited from an occupied state to an unoccupied state, that is, it creates a hole in the Fermi sea and a particle above

https://doi.org/10.1017/9781108489065.015 Published online by Cambridge University Press

the sea. This is known as $1p-1h$ excitation, with the condition that the initial momentum: $|\vec{p}| < |\vec{p}_F^{\,i}|$ and the final momentum: $|\vec{p}+\vec{q}| > |\vec{p}_F^{\,i}|$. This condition is incorporated in the expression (Eq. 14.7) for the free nucleon cross section for the scattering of (anti)neutrinos from the free nucleon at rest.

Inside the nucleus

$$\left.\frac{d^2\sigma_{\nu l}}{d\Omega(\hat{k}')dE_l'}\right|_{\text{Nucleus}} = \frac{G_F^2\cos^2\theta_C}{128\pi^2}\int \frac{1}{E_nE_p}2d\vec{p}\,\frac{1}{(2\pi)^3}n_n(\vec{p})(1-n(|\,\vec{p}+\vec{q}\,|)\frac{|\vec{k}'|}{|\vec{k}\,|}\delta(q_0+E_n-E_p)L_{\mu\nu}J^{\mu\nu}. \tag{14.65}$$

The hadronic tensor $J_{\mu\nu}$ has to be integrated over the Fermi momentum of the initial nucleon subject to the aforementioned conditions, that is, $J_{\mu\nu}$ is replaced by

$$\begin{aligned}
\frac{M^2}{E_nE_p}J_{\mu\nu}\delta(q_0+E_n-E_p) \quad &\longrightarrow \quad \int f(q,p)J_{\mu\nu}(p)\frac{d^3p}{(2\pi)^3}f(q,p) \\
f(q,p) \quad &= \quad n(|\,\vec{p}\,|)(1-n(|\,\vec{p}+\vec{q}\,|)\frac{M^2}{E_nE_p}\delta(q_0+E_n-E_p) \\
n(|\,\vec{p}\,|) \quad &= \quad \theta(p_F^i-p) \text{ and } (1-n(|\,\vec{p}+\vec{q}\,|) = \theta(|\,\vec{p}+\vec{q}\,|-p_F^f).
\end{aligned} \tag{14.66}$$

$J_{\mu\nu}$ involves terms like $g_{\mu\nu}, q_\mu q_\nu, p_\mu p_\nu$, and $p_\mu q_\nu$.

Now, $\int f(q,p)J_{\mu\nu}(p)\,\frac{d^3p}{(2\pi)^3}$ can be evaluated explicitly.

These are the main features of the Smith and Moniz relativistic Fermi gas (RFG) model.

Gaisser and O'Connell [658] have used the relativistic response function $R(\vec{q},q_0)$,

in a Fermi gas model to take into account nuclear medium effects. The expression for the double differential scattering cross section is given by

$$\begin{aligned}
\left(\frac{d^2\sigma}{d\Omega_l dE_l}\right)_{(\nu/\bar{\nu})} \quad &= \quad C\left(\frac{d\sigma_{\text{free}}}{d\Omega_l}\right)_{(\nu/\bar{\nu})}R(\vec{q},q_0), \\
R(\vec{q},q_0) \quad &= \quad \frac{1}{\frac{4}{3}\pi p_{F_N}^3}\int \frac{d^3p_N\,M^2}{E_NE_{N'}}\delta(E_N+q_0-E_B-E_{N'})\theta(p_{F_N}-|\vec{p}_N|) \\
&\times \quad \theta(|\vec{p}_N+\vec{q}|-p_{F_{N'}}), \\
\left(\frac{d\sigma_{\text{free}}}{d\Omega_l}\right)_{(\nu/\bar{\nu})} \quad &= \quad \frac{G_F^2k'E_l}{2\pi^2}\Bigg\{(f_1^2+g_1^2+Q^2f_2^2)\cos^2\frac{\theta}{2}+2\left[g_1^2\left[1+\frac{Q^2}{4M^2}\right]\right. \\
&+ \quad \left.\frac{Q^2}{4M^2}\mu^2f_1^2\right]\sin^2\frac{\theta}{2}\mp\frac{2g_1}{M}f_1\mu\left[Q^2+q_0^2\sin^2\frac{\theta}{2}\right]^{\frac{1}{2}}\sin\frac{\theta}{2}\Bigg\},
\end{aligned} \tag{14.67}$$

where $Q^2 = -q^2 = -(k-k')^2$ and p_{F_N} is the Fermi momentum for the initial nucleon, $N, N' = n$ or p and $C = A-Z$ for a neutrino induced process and $C = Z$ for an antineutrino induced process.

14.5.3 Local Fermi gas model

In the local Fermi gas (LFG) model, the Fermi momenta of the initial and final nucleons are not constant, but depend upon the interaction point $\vec{r}$ and are bounded by their respective Fermi

https://doi.org/10.1017/9781108489065.015 Published online by Cambridge University Press

momentum at r, that is, $p_{F_n}(r)$ and $p_{F_p}(r)$ for neutron and proton, respectively, where $p_{F_n}(r) = \left[3\pi^2\rho_n(r)\right]^{\frac{1}{3}}$ and $p_{F_p}(r) = \left[3\pi^2\rho_p(r)\right]^{\frac{1}{3}}$, $\rho_n(r)$ and $\rho_p(r)$ being the local neutron and proton nuclear densities, respectively. The proton density is expressed in terms of the nuclear charge density $\rho(r)$ as $\rho_p(r) = \frac{Z}{A}\rho(r)$ and the neutron density is given by $\rho_n(r) = \frac{A-Z}{A}\rho(r)$, where $\rho(r)$ is the nuclear density, determined experimentally by the electron–nucleus scattering experiments [682, 683] for the proton and neutron matter density is obtained using the Hartree–Fock calculation.

In the local density approximation, the cross section is evaluated as a function of the local Fermi momentum, $p_F(r)$ and integrated over the whole nucleus. The differential scattering cross section is given as

$$\left(\frac{d\sigma}{d\Omega_l dE_l}\right)_{\nu A} = \int \rho_n(r) d^3r \left(\frac{d\sigma}{d\Omega_l dE_l}\right)_{\nu N}, \tag{14.68}$$

where

$$\left(\frac{d\sigma}{d\Omega_l dE_l}\right)_{\nu N} = \frac{|\vec{k'}|}{64\pi^2 E_\nu M_n M_p} \overline{\sum}\sum |\mathcal{M}|^2 \frac{M_n M_p}{E_n E_p} \delta(E_\nu + E_n(p) - E_l - E_p), \tag{14.69}$$

is the differential scattering cross section for the free neutrino nucleon scattering.

The modified harmonic oscillator (MHO) density

$$\rho(r) = \rho(0)\left[1 + a\left(\frac{r}{R}\right)^2 \exp\left[-\left(\frac{r}{R}\right)^2\right]\right] \tag{14.70}$$

for ^{12}C and ^{16}O and the two-parameter Fermi density (2 pF)

$$\rho(r) = \frac{\rho(0)}{\left[1 + \exp\left(\frac{r-R}{a}\right)\right]} \tag{14.71}$$

for ^{40}Ar, ^{56}Fe, and ^{208}Pb with R and a as density parameters have been used in many calculations. In Table 14.2, we show the nuclear density and other parameters needed for the numerical calculations in this chapter. In Figure 14.6, we have shown the Fermi momentum ($p_F(r)$) as a function of position (r) for various nuclei.

Fermi motion and binding energy

In a symmetric nuclear matter, each nucleon occupies a volume of $(2\pi)^3$. However, because of two possible spin orientations of nucleons, each unit cell in configuration space is occupied by two nucleons. Thus, the number of nucleons N in a certain volume V is

$$N = 2V \int^{p_F} \frac{d^3p}{(2\pi)^3} n_n(p,r) d^3r \tag{14.72}$$

$$\text{or } \rho(r) = \frac{N}{V} = 2\int \frac{d^3p}{(2\pi)^3} n_n(p,r), \tag{14.73}$$

https://doi.org/10.1017/9781108489065.015 Published online by Cambridge University Press

Table 14.2 Binding energy, and Q value of the reaction for various nuclei. The last three columns are the parameters for MHO and 2pF densities. * is dimensionless for the MHO density.

Nucleus	Binding energy (MeV)	Q value (ν) (MeV)	Q value ($\bar{\nu}$) (MeV)	R_p (fm)[660]	R_n (fm)[660]	a (fm)*[660]
^{12}C	25	17.84	13.90	1.69	1.692	1.082(MHO)
^{16}O	27	19.70	14.30	1.83	1.833	1.544(MHO)
^{40}Ar	30	3.64	8.05	3.47	3.64	0.569(2pF)
^{56}Fe	36	6.52	4.35	3.97	4.05	0.593(2pF)
^{208}Pb	44	5.20	5.54	6.62	6.89	0.549(2pF)

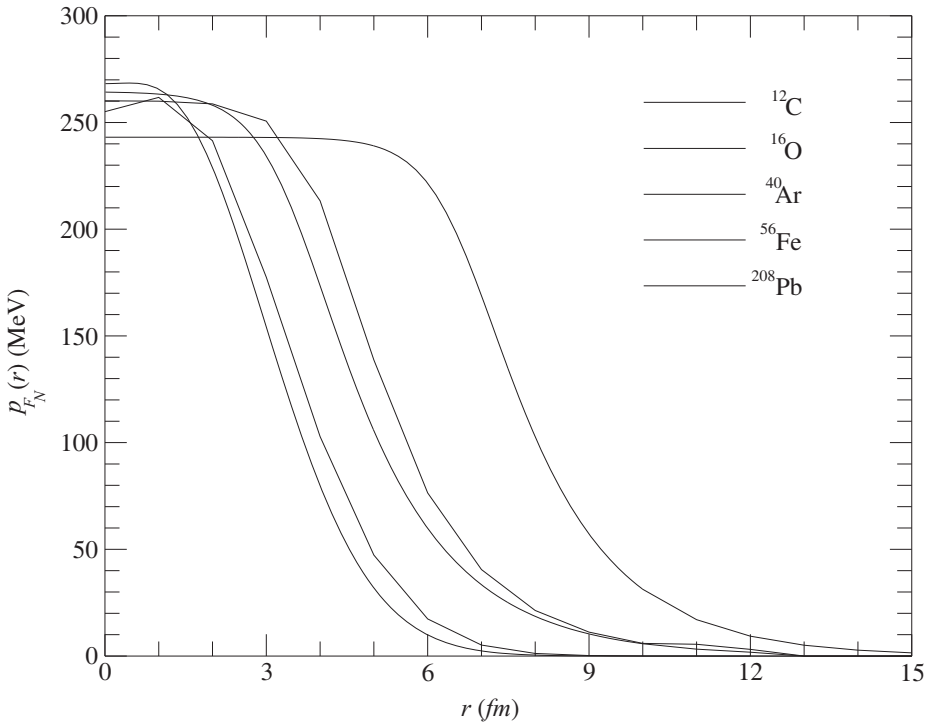

Figure 14.6 Fermi momentum $p_F(r)$ versus r for various nuclei.

where $n_N(\vec{p},r)$ $(N = n,p)$ is the local occupation number for the nucleon. The initial nucleon has $n_i(\vec{p},r)$= 1 for $p < p_F(r)$, where $p_F(r)$ is the maximum momentum called the Fermi momentum at position $\vec{r}$. The factor 2 in Eq. (14.72) is due to the spin degree of freedom of the nucleons.

Thus, using Eqs. (14.73) and (14.69) in Eq. (14.68), we obtain for $\nu_l n \to l^- p$ scattering process

$$\left(\frac{d\sigma}{d\Omega_l dE_l}\right)_{\nu A} = 2\int\int d^3r \frac{d^3p}{(2\pi)^3} n_n(p,r) \left(\frac{d\sigma}{d\Omega_l dE_l}\right)_{\nu N}$$

https://doi.org/10.1017/9781108489065.015 Published online by Cambridge University Press

$$= 2\int\int d^3r \frac{d^3p}{(2\pi)^3} n_n(p,r) \frac{|\vec{k}'|}{64\pi^2 E_\nu M_n M_p} \overline{\sum}\sum |\mathcal{M}|^2 \frac{M_n M_p}{E_n E_p}$$
$$\times \delta(E_\nu(\vec{k}) + E_n(\vec{p}) - E_l(\vec{k}') - E_p(\vec{p}')). \tag{14.74}$$

Instead of using Eq. (14.74), we use the methods of the many-body field theory [684] where

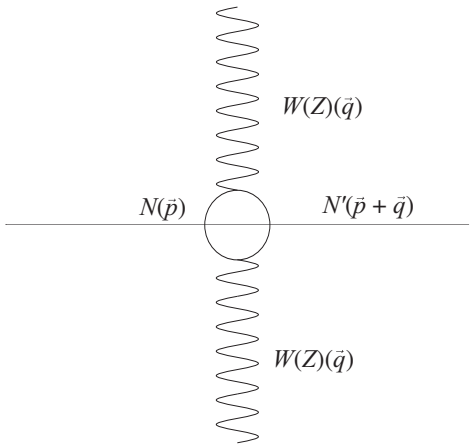

Figure 14.7 Diagrammatic representation of the particle–hole $(p-h)$ excitation induced by $W(Z)$ boson in the large mass limit of intermediate vector boson $(M_{W(Z)} \to \infty)$.

the reaction cross section for the process $\nu_l + n \to l^- + p$ in a nuclear medium is given in terms of the imaginary part of the Lindhard function Im $U_N(q_0, \vec{q})$ [639, 684] corresponding to the particle–hole $(1p-1h)$ excitation diagram shown in Figure 14.7. This can be done by replacing the factor

$$-2\pi \int \frac{d^3p}{(2\pi)^3} n_n(p,r) \frac{M_n M_p}{E_n E_p} \delta(E_\nu(\vec{k}) + E_n(\vec{p}) - E_l(\vec{k}') - E_p(\vec{p}')) \tag{14.75}$$

by the imaginary part of the Lindhard function Im $U_N(q_0, \vec{q})$. Now the cross section is evaluated using Eq. (14.75) in Eq. (14.74). This is permissible if we assume an average value of $|\vec{p}\,|^2$ in $|\mathcal{M}|^2$ in the nuclear medium corresponding to the Fermi energy of the nucleons. Thus, d^3p integration is performed and the results are written in terms of the Lindhard function given in Eq. (14.76) corresponding to the particle–hole excitation given by (Figure 14.7):

$$U_N(q_0, \vec{q}) = 2\int \frac{d^3p_n}{(2\pi)^3} \frac{M_n M_p}{E_n E_p} \frac{n_n(\vec{p})\left[1 - n_p(\vec{p}+\vec{q})\right]}{q_0 + E_n(\vec{p}) - E_p(\vec{p}+\vec{q}) + i\epsilon'}, \tag{14.76}$$

Taking the imaginary part of the Lindhard function in Eq. (14.76) corresponds to putting the intermediate particles in Figure 14.7 on shell, thereby describing the process $\nu_l + n \to l^- + p$. In the static limit for the neutron $(E_n \to M_n)$ and neglecting any Pauli blocking for the proton $(n_p \to 0)$, one recovers the result for the free nucleons.

https://doi.org/10.1017/9781108489065.015 Published online by Cambridge University Press

To evaluate the imaginary part of the Lindhard function (Eq. (14.76)), we use the following relation

$$\frac{1}{\omega \pm i\eta} = \mathcal{P}\frac{1}{\omega} \mp i\pi\delta(\omega), \tag{14.77}$$

which results in

$$\mathrm{Im}(U_N(q_0,\vec{q})) = -2\pi \int \frac{d^3p_n}{(2\pi)^3}\, n_n(\vec{p})\,[1-n_p(\vec{p}+\vec{q})]\,\delta(q_0+E_n-E_p)\,\frac{M_pM_n}{E_pE_n}, \tag{14.78}$$

where $n_n(\vec{p})$ is the occupation number. Since $\vec{q} = \vec{p}' - \vec{p}$, we have

$$\begin{aligned} E_p &= \sqrt{(\vec{p}+\vec{q})^2+M^2} = \sqrt{|\vec{p}|^2+|\vec{q}|^2+2|\vec{p}||\vec{q}|\cos\theta+M^2} \\ \text{and } E_n &= \sqrt{|\vec{p}|^2+M^2}. \end{aligned} \tag{14.79}$$

Using $n_n(\vec{p}) = 1$ for $p \le p_{F_n}$, we evaluate Eq. (14.78) to obtain

$$\begin{aligned} \text{Im } U_N(q_0,\vec{q}) = -(2\pi)^2 M_pM_n \int_0^{p_{F_n}} \frac{|\vec{p}_n|^2 d|\vec{p}_n|}{(2\pi)^3}\,\frac{[1-n_p(\vec{p}+\vec{q})]}{\sqrt{|\vec{p}|^2+M^2}} \int_{-1}^{1} d(\cos\theta) \\ \Big(\frac{1}{\sqrt{|\vec{p}|^2+|\vec{q}|^2+2|\vec{p}||\vec{q}|\cos\theta+M^2}}\Big) \\ \delta\Big(q_0+\sqrt{|\vec{p}|^2+M^2}-\sqrt{|\vec{p}|^2+|\vec{q}|^2+2|\vec{p}||\vec{q}|\cos\theta+M^2}\Big). \end{aligned} \tag{14.80}$$

Using the δ function property,

$$\int f(x)\delta\,[g(x)]\,dx = \int f(x)\frac{\delta\,[g(x)]}{g'(x)}dg(x) = \sum_i \frac{f(x)}{|\partial g(x_i)/\partial x|}, \tag{14.81}$$

where

$$f(x) = \frac{1}{\sqrt{|\vec{p}|^2+|\vec{q}|^2+2|\vec{p}||\vec{q}|cos\theta+M^2}}, \tag{14.82}$$

$$g(x) = q_0+\sqrt{|\vec{p}|^2+M^2}-\sqrt{|\vec{p}|^2+|\vec{q}|^2+2|\vec{p}||\vec{q}|cos\theta+M^2}, \tag{14.83}$$

with $x = \cos\theta$. The points x_i are the real roots of $g(x) = 0$ in the interval of integration, that is,

$$q_0+\sqrt{|\vec{p}|^2+M^2} = \sqrt{|\vec{p}|^2+|\vec{q}|^2+2|\vec{p}||\vec{q}|cos\theta+M^2}.$$

The $\cos\theta$ integral can be performed.

$$\cos\theta = \frac{q_0^2-|\vec{q}|^2+2q_0\sqrt{|\vec{p}|^2+M^2}}{2|\vec{p}||\vec{q}|} \le 1. \tag{14.84}$$

https://doi.org/10.1017/9781108489065.015 Published online by Cambridge University Press

Further,

$$[1 - n_p(\vec{p} + \vec{q})] = \Theta(|\vec{p} + \vec{q}| - p_{F_p}) \;\; \Rightarrow \;\; (\vec{p} + \vec{q})^2 > p_{F_p}^2.$$

Using the expression for $\cos\theta$, this expression becomes

$$\sqrt{q_0^2 - |\vec{p}|^2 + 2q_0\sqrt{|\vec{p}|^2 + M^2}} > p_{F_p}. \tag{14.85}$$

Thus, the expression for the Lindhard function(Eq. (14.80)) is obtained as:

$$\begin{aligned} \mathrm{Im}(U_N(q_0, \vec{q})) &= \frac{M_p M_n}{2\pi} \int_0^{p_{F_n}} \frac{d|\vec{p}|}{\sqrt{|\vec{p}|^2 + M^2}} \frac{|\vec{p}|}{|\vec{q}|} \Theta(1 - |\cos\theta|)\, \Theta(A_1 - p_{F_2}) \\ &= \frac{M_p M_n}{2\pi} \int_0^{p_{F_n}} \frac{dE}{|\vec{q}|} \Theta(1 - |\cos\theta|)\, \Theta(A_1 - p_{F_2}). \end{aligned} \tag{14.86}$$

Applying the kinematical constraint discussed earlier, we may re-write Eq. (14.86) as

$$\mathrm{Im}\, U_N(q_0, \vec{q}) = -\frac{1}{2\pi} \frac{M_p M_n}{|\vec{q}|} \left[E_{F_1} - A\right] \quad \text{with} \tag{14.87}$$

$$q^2 < 0, \;\; E_{F_2} - q_0 < E_{F_1} \text{ and } \frac{-q_0 + |\vec{q}|\sqrt{1 - \frac{4M^2}{q^2}}}{2} < E_{F_1}, \tag{14.88}$$

where

$$\begin{aligned} E_{F_1} &= \sqrt{{p_{F_n}}^2 + {M_n}^2}, \;\; E_{F_2} = \sqrt{{p_{F_p}}^2 + {M_p}^2} \text{ and} \\ A &= \mathrm{Max}\left[M_n,\, E_{F_2} - q_0,\, \frac{-q_0 + |\vec{q}|\sqrt{1 - \frac{4M^2}{q^2}}}{2}\right]. \end{aligned} \tag{14.89}$$

Otherwise, $\mathrm{Im}(U_N(q_0, \vec{q})) = 0$.

The energies E_n and E_p of the neutron and proton in the Lindhard function refers to the local Fermi sea of the nucleons in the initial and final nucleus. In the Fermi sea, there is no energy gap between the occupied and unoccupied states; therefore, particle–hole($1p - 1h$) excitations can be produced with an infinitesimal energy. However, in case of finite nuclei, this is not the case. In finite nuclei, there exists a certain energy gap between the ground state of initial and final nuclei. This is the minimum excitation energy needed for transition to the ground state of the final nucleus. It is also the threshold energy (Q_{th}) of the reaction. Therefore, in nuclei, the correction due to the threshold value of the reaction Q_{th} (Table 14.2) has to be taken into account in order to get a reliable value of the cross section, specially for low energy neutrinos.

This threshold energy Q_{th} of the nuclear reactions is incorporated in these calculations by replacing the energy conserving δ function, that is, $\delta[q_0 + E_n - E_p]$ in Eq. (14.74) by $\delta[q_0 + E_n(\vec{p}) - E_p(\vec{p} + \vec{q}) - Q_{th}]$ and evaluating the Lindhard function $q_0 - Q_{th}$ instead of

https://doi.org/10.1017/9781108489065.015 Published online by Cambridge University Press

q_0. Moreover, to account for the unequal Fermi sea for neutrons and protons for $N \neq Z$ nuclei, the factor $Q'_{th} = E_{Fn} - E_{Fp}$ is added to q_0 in the Lindhard function. Thus, q_0 is replaced by $q_0 - Q_{th} + Q'_{th} = E_\nu - E_l - Q_{th} + Q'_{th}$ in the Lindhard function. Because of its nature, this method only applies to inclusive processes by summing over relatively many final states. The implementation of this modification to perform numerical evaluation of cross sections requires a reasonable choice for threshold value of the nuclear reaction Q_{th}. The value of Q_{th}, for the neutrino reaction is generally taken to be the energy difference corresponding to the lowest allowed Fermi or Gamow–Teller transitions.

With the inclusion of these nuclear effects, the neutrino nuclear cross section $\sigma(E_\nu)$ is written as

$$\begin{aligned}\sigma(E_\nu) &= -\frac{G_F^2 \cos^2\theta_C}{32\pi} \int_{r_{\min}}^{r_{\max}} r^2 dr \int_{k'\min}^{k'\max} k'^2 dk' \int_{-1}^{1} d(\cos\theta) \frac{1}{E_{\nu_e} E_e} \\ &\quad \times L^{\mu\nu} J_{\mu\nu}\, \mathrm{Im} U_N[E_\nu - E_l - Q_{th}, \vec{q}\,]. \end{aligned} \tag{14.90}$$

Coulomb correction

One of the important aspects of charge current neutrino interactions is the treatment of Coulomb distortion of the produced lepton in the Coulomb field of the final nucleus. At low energies of the electron relevant to β decays in the nuclei, the Coulomb distortion of electrons in the nuclear field is taken into account by multiplying the momentum distribution of the electron by a Fermi function $F(Z, E_e)$, where $F(Z, E_e)$ is given by:

$$F(Z, E_e) = \left[1 - \frac{2}{3}(1 - \gamma_0)\right]^{-1} f(Z, E_e),$$

with

$$f(Z, E_e) = 2(1 + \gamma_0))(2p_e R)^{-2(1-\gamma_0)} \frac{|\Gamma(\gamma_0 + i\eta)|^2}{(\Gamma(2\gamma_0 + 1))^2}.$$

Here, R is the nuclear radius and $\gamma_0 = \sqrt{1 - (\alpha Z)^2}$, $\eta = \frac{\alpha Z c}{v}$. This approximation works quite well at low energies, but it is not appropriate at higher energies, especially for high Z nuclei [685]. Therefore, at higher electron energies, a different approach is needed to describe the Coulomb distortion effect of the electron. For this purpose, we apply the methods used in electron scattering where various approximations have been used to take into account the Coulomb distortion effects of the initial and final electron. One of them is the modified effective momentum approximation (MEMA) in which the electron momentum and energy are modified by taking into account the Coulomb energy [685].

The Coulomb distortion effect on the outgoing lepton has been taken into account in MEMA in which the lepton momentum and energy are modified by replacing E_l with $E_l + V_c(r)$. The form of Coulomb potential $V_c(r)$ considered here is [686]:

$$V_c(r) = Z_f \alpha\, 4\pi \left(\frac{1}{r} \int_0^r \frac{\rho_p(r')}{Z} r'^2 dr' + \int_r^\infty \frac{\rho_p(r')}{Z} r' dr' \right), \tag{14.91}$$

https://doi.org/10.1017/9781108489065.015 Published online by Cambridge University Press

where α is a fine structure constant(1/137.035), Z_f is the charge of the outgoing lepton which is –1 in the case of neutrino and +1 in the case of antineutrino. $\rho_p(r)(\rho_n(r))$ is the proton(neutron) density of the final nucleus.

Incorporation of these considerations results in modification in the argument of the Lindhard function, that is,

$$\mathrm{Im}U_N(q_0^{\nu(\bar{\nu})}, |\vec{q}|) \longrightarrow \mathrm{Im}U_N(q_0^{\nu(\bar{\nu})} - V_c(r), \vec{q}).$$

With the inclusion of these nuclear effects, the cross section $\sigma(E_\nu)$ is written as

$$\begin{aligned}\sigma(E_\nu) &= -\frac{G_F^2\cos^2\theta_C}{32\pi}\int_{r_{\min}}^{r_{\max}} r^2dr\int_{k'_{\min}}^{k'_{\max}} k'^2dk'\int_{-1}^{1} d\cos(\theta)\frac{1}{E_{\nu_l}^2E_l}L_{\mu\nu}J^{\mu\nu}\\ &\times\mathrm{Im}U_N(q_0^{\nu(\bar{\nu})} - V_c(r), \vec{q}).\end{aligned} \tag{14.92}$$

Thus, in the presence of nuclear medium effects, the total cross section $\sigma(E_\nu)$, with the inclusion of Coulomb distortion effects taken into account by the Fermi function (MEMA), is written as

$$\begin{aligned}\sigma^{FF(MEMA)}(E_\nu) = -\frac{G_F^2\cos^2\theta_C}{32\pi}\int_{r_{\min}}^{r_{\max}} r^2dr\int_{k_{\min'}}^{k_{\max'}} k'^2dk'\int_{-1}^{1} d(\cos\theta)\\ \times\frac{1}{E_{\nu_e}E_e}L_{\mu\nu}J^{\mu\nu}_{RPA}ImU_N{}^{FF(MEMA)},\end{aligned} \tag{14.93}$$

where

$$\begin{aligned}ImU_N^{FF} &= F(Z,E_e)ImU_N[E_{\nu_e} - E_e - Q, \vec{q}] \text{ and}\\ ImU_N^{MEMA} &= ImU_N[E_{\nu_e} - E_e - Q - V_c(r), \vec{q}], \quad Q = Q_{th} + Q'_{th}.\end{aligned} \tag{14.94}$$

Nucleon–nucleon correlations and random phase approximation

In nuclei, the strength of the electroweak couplings may not be the same as their free nucleon values due to the presence of strongly interacting nucleons. Though the conservation of vector current (CVC) forbids any change in the charge coupling, other couplings like magnetic, axial charge, and pseudoscalar couplings are likely to change from their free nucleon values. Due to PCAC, the axial current is strongly coupled to the pion field in the nuclear medium and therefore, axial couplings are more likely to change due to pionic effects modifying the nuclear response functions. To get an idea of these effects, we perform a nonrelativistic reduction of the hadronic current(J_μ given in Chapter 10). We see the occurrence of $g_1\vec{\sigma}\vec{\tau}$, $f_2\vec{\sigma}\times\vec{q}\vec{\tau}$, and $g_3\vec{\sigma}\cdot\vec{q}\vec{\tau}$ terms (Appendix A) in the weak current which are linked to the spin isospin excitation; f_2 and g_3 are coupled to the transverse and longitudinal channels. g_1 is coupled to both. There exists considerable work in understanding the quenching of magnetic moment and axial charge in nuclei due to the nucleon–nucleon correlations. In our approach, the nucleon–nucleon correlation effects are reflected in the modification of the nuclear response in longitudinal and transverse channels. We calculate this reduction in the vector–axial (VA) and axial–axial (AA) response functions due to the long range nucleon–nucleon correlations treated in the RPA, diagrammatically shown in Figure 14.8.

https://doi.org/10.1017/9781108489065.015 Published online by Cambridge University Press

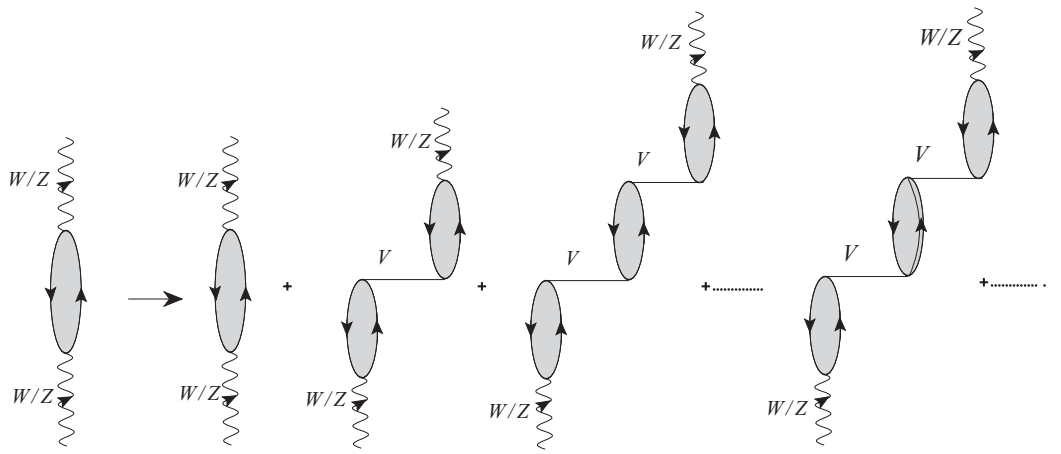

Figure 14.8 RPA effects in the $1p-1h$ contribution to the W/Z self-energy, where particle–hole, Δ–hole, Δ–Δ, etc. excitations contribute.

The diagram shown in Figure 14.8 simulates the effects of the strongly interacting nuclear medium at the weak vertex. The $ph-ph$ interaction is shown by the dashed line and is described by the π and ρ exchanges modulated by the effect of short range correlations. For the $ph-ph$ potential, we use

$$V_N(q) = V_\pi(q) + V_\rho(q) \tag{14.95}$$

with the potential corresponding to πNN interaction which gives longitudinal part of the interaction and is defined as:

$$V_\pi(q) = \left(\frac{f_\pi^2}{m_\pi^2}\right) |\vec{q}|^2 \left[\frac{\hat{q}_i\hat{q}_j\sigma_i\sigma_j}{q_0^2 - \vec{q}^2 - m_\pi^2 + i\epsilon}\right] \vec{\tau}\cdot\vec{\tau} \tag{14.96}$$

and the ρNN interaction gives the transverse part of interaction which is given by

$$V_\rho(q) = \left(\frac{f_\rho^2}{m_\rho^2}\right) |\vec{q}|^2 \left[\frac{(\delta_{ij} - \hat{q}_i\hat{q}_j)\sigma_i\sigma_j}{q_0^2 - \vec{q}^2 - m_\rho^2 + i\epsilon}\right] \vec{\tau}\cdot\vec{\tau}, \tag{14.97}$$

where f_π and f_ρ are the coupling strengths and $\frac{f_\pi^2}{4\pi} = 0.08$, $\frac{f_\rho^2}{m_\rho^2} = 2\frac{f_\pi^2}{m_\pi^2}$. $V_\pi(q)$+$V_\rho(q)$ provides the spin-isospin part of the nucleon-nucleon interaction in the meson exchange model. Therefore, $V_N(q)$ may be expressed as

$$V_N(q) = \frac{f^2}{m_\pi^2}\left[V_t(q)(\delta_{ij} - \hat{q}_i\hat{q}_j) + V_l(q)\hat{q}_i\hat{q}_j\right](\sigma_i\sigma_j)(\vec{\tau}\cdot\vec{\tau}) \tag{14.98}$$

https://doi.org/10.1017/9781108489065.015 Published online by Cambridge University Press

for the ph case and a similar potential V_Δ is obtained in the case of $ph - \Delta h$ interaction by substituting $\vec{\sigma} \to \vec{S}$, $\vec{\tau} \to \vec{T}$, and $f \to f^* = 2.15f$. V_l is the strength of the potential in the longitudinal channel and V_t is the strength of the potential in the transverse channel. The representation into longitudinal and transverse channels is useful when one tries to sum the geometric series in Figure 14.8 where the longitudinal and transverse channels decouple and can be summed independently.

The potential $V(q)$ due to π and ρ exchange is explicitly written as:

$$V_l(q) = \frac{f^2}{m_\pi^2}\left[\frac{q^2}{-q^2+m_\pi^2}\left(\frac{\Lambda_\pi^2 - m_\pi^2}{\Lambda_\pi^2 - q^2}\right)^2 + g'\right],$$
$$V_t(q) = \frac{f^2}{m_\pi^2}\left[\frac{q^2}{-q^2+m_\rho^2}C_\rho\left(\frac{{\Lambda_\rho}^2 - m_\rho^2}{{\Lambda_\rho}^2 - q^2}\right)^2 + g'\right]. \tag{14.99}$$

$\frac{f^2}{4\pi} = 0.8$, $\Lambda_\pi = 1.3$ GeV, $C_\rho = 2$, $\Lambda_\rho = 2.5$ GeV, m_π and m_ρ are the pion and rho meson masses, and g' is the Landau–Migdal parameter taken to be 0.7 which has been used quite successfully to explain many electromagnetic and weak processes in nuclei [641, 687, 688].

Using the matrix elements at the weak WNN vertex and the $ph - ph$ potential, the contribution of Figure 14.8 is written as

$$U(q) = U(q) + U(q)V_N(q)U(q) + U(q)V_N(q)U(q)V_N(q)U(q) + ... \tag{14.100}$$

Writing the potential $V_N(q)$ in terms of V_l and V_t, the series in Eq. (14.100) can be separated into the longitudinal and transverse components using the following relationship:

$$\left.\begin{array}{l}(\delta_{ij} - \hat{q}_i\hat{q}_j)(\delta_{jl} - \hat{q}_j\hat{q}_l) = \delta_{il} - \hat{q}_i\hat{q}_l \\ \hat{q}_i\hat{q}_j\hat{q}_j\hat{q}_l = \hat{q}_i\hat{q}_l \\ (\delta_{ij} - \hat{q}_i\hat{q}_j)\hat{q}_j\hat{q}_l = 0\end{array}\right\}. \tag{14.101}$$

The longitudinal part is then written as

$$\begin{aligned} U_L(q) &= \left[U(q) + U(q)V_l\hat{q}_i\hat{q}_j\sigma_i\sigma_j U(q) + U(q)V_l\hat{q}_i\hat{q}_k\sigma_i\sigma_k U(q)V_l\hat{q}_k\hat{q}_j\sigma_k\sigma_j U(q) + ...\right]\ \vec{\tau}_1\cdot\vec{\tau}_2 \\ &= [U(q) + U(q)V_l U(q) + U(q)V_l U(q)V_l U(q) + ...]\ \hat{q}_i\hat{q}_j\ \sigma_i\sigma_j\ \vec{\tau}_1\cdot\vec{\tau}_2 \\ &= U(q)[1 + V_l U(q) + (V_l U(q))^2 + ...]\ \hat{q}_i\hat{q}_j\ \sigma_i\sigma_j\ \vec{\tau}_1\cdot\vec{\tau}_2 \\ &= \left[\frac{U(q)}{1 - U(q)V_l}\right]\ \hat{q}_i\hat{q}_j\ \sigma_i\sigma_j\ \vec{\tau}_1\cdot\vec{\tau}_2. \end{aligned} \tag{14.102}$$

Similarly, the transverse part is given by

$$U_T(q) = \left[\frac{U(q)}{1 - U(q)V_t}\right]\ (\delta_{ij} - \hat{q}_i\hat{q}_j)\ \sigma_i\sigma_j\ \vec{\tau}_1\cdot\vec{\tau}_2. \tag{14.103}$$

Therefore, we can write Eq. (14.100) as:

$$\bar{U}(q) = \left[\left(\frac{U(q)}{1 - U(q)V_t}\right)\ (\delta_{ij} - \hat{q}_i\hat{q}_j) + \left(\frac{U(q)}{1 - U(q)V_l}\right)\ \hat{q}_i\hat{q}_j\right]\ \vec{\sigma}_i\ \vec{\sigma}_j\vec{\tau}_1\cdot\vec{\tau}_2, \tag{14.104}$$

https://doi.org/10.1017/9781108489065.015 Published online by Cambridge University Press

where $U = U_N + U_\Delta$, with U_N and U_Δ as the Lindhard function for particle–hole$(1p-1h)$ and Δh excitations, respectively, in the medium. The expressions for U_N and U_Δ are taken from Ref. [689].

To demonstrate how these renormalizations are done, we demonstrate it for a few cases. like the renormalization of the axial vector term of the hadronic current in Chapter 10. The nonrelativistic reduction of the axial vector term is written as

$$\begin{aligned}\bar{u}(p')g_1(q^2)\gamma_\mu\gamma_5 u(p) &= (J_0,\, J_i) = g_1(q^2)\left[\bar{u}(p')\gamma_0\gamma_5 u(p),\ \bar{u}(p')\gamma_i\gamma_5 u(p)\right] \\ &= g_1(q^2)\left[\frac{\sigma_i\cdot(\vec{p}+\vec{p'})}{2E},\quad \left(\sigma_i + \frac{\sigma_i(\vec{\sigma}\cdot\vec{p})(\vec{\sigma}\cdot\vec{p'})}{4E^2}\right)\right] \quad (14.105)\end{aligned}$$

Similarly, considering the term

$$\bar{u}(p')\, f_1(q^2)\, \gamma_\mu\, u(p),$$

we get

$$f_1(q^2)\,\bar{u}(p')\,\gamma_0\,u(p) = f_1(q^2)\left[1 + \frac{|\vec{p}|^2 + i\epsilon_{ijk}\,p_i p_j\sigma_k + \vec{p}\cdot\vec{q} + i\epsilon_{ijk}\,q_i p_j\sigma_k}{(2M)^2}\right] \quad (14.106)$$

and

$$f_1(q^2)\,\bar{u}(p')\,\gamma_i\,u(p) = f_1(q^2)\frac{1}{2M}\left[(2p_i+q_i) - i\epsilon_{ijk}\,q_j\sigma_k\right]. \quad (14.107)$$

Now collecting J_0 and J_i terms together of the hadronic current J_μ, we get

$$J_0 = \frac{g_1(q^2)}{2M}\,\sigma_i P_i + f_1(q^2)\left[1 + \frac{\vec{p}\cdot\vec{p'} + i\epsilon_{ijk}\,p'_i p_j\sigma_k}{(2M)^2}\right] + \frac{f_2(q^2)}{(2M)^2}\,\sigma_l q_l \sigma_m q_m \quad (14.108)$$

and

$$J_i = g_1(q^2)\left[\sigma_i + \frac{\sigma_i(\vec{\sigma}\cdot\vec{p})(\vec{\sigma}\cdot\vec{p'})}{(2M)^2}\right] + \frac{f_1(q^2)}{2M}\left[P_i - i\epsilon_{ijk}\,q_j\sigma_k\right] - i\frac{f_2(q^2)}{2M}\,\epsilon_{jkl}\sigma_k q_l, \quad (14.109)$$

which leads to

$$\begin{aligned}J_{00} &= \bar{\sum}\sum\left\{\frac{g_1(q^2)}{2M}\,\sigma_i P_i + f_1(q^2)\left[1 + \frac{\vec{p}\cdot\vec{p'} + i\epsilon_{ilm}\,p'_i p_l\sigma_m}{(2M)^2}\right] + \frac{f_2(q^2)}{(2M)^2}\,\sigma_l q_l\sigma_m q_m\right\} \\ &\quad\times\left\{\frac{g_1(q^2)}{2M}\sigma_j P_j + f_1(q^2)\left[1 + \frac{\vec{p}\cdot\vec{p'} + i\epsilon_{jl'm'}\,p'_j p_{l'}\sigma_{m'}}{(2M)^2}\right] + \frac{f_2(q^2)}{(2M)^2}\sigma_{l'}q_{l'}\sigma_{m'}q_{m'}\right\}. \quad (14.110)\end{aligned}$$

Neglecting the terms with $1/(2M)^3$, $1/(2M)^4$ or higher powers and using the trace relations given in Appendix C, we finally get

$$J_{00} = \left[\left(\frac{g_1(q^2)}{2M}\right)^2\sigma_i P_i\sigma_j P_j + (f_1(q^2))^2\left\{1 + \frac{2\vec{p}\cdot\vec{p'}}{(2M)^2}\right\} + 2\frac{f_1(q^2)f_2(q^2)}{(2M)^2}\sigma_l q_l\sigma_l\sigma_m\right],$$

https://doi.org/10.1017/9781108489065.015 Published online by Cambridge University Press

$$= \left[2\left(\frac{g_1(q^2)}{2M}\right)^2 \vec{P}^2 + 2(f_1(q^2))^2\left\{1+\frac{2\vec{p}\cdot(\vec{p}+\vec{q})}{(2M)^2}\right\} + 4\frac{f_1(q^2)f_2(q^2)}{(2M)^2}|\vec{q}|^2\right]. \quad (14.111)$$

Now we evaluate the expression for J_{0i}

$$\begin{aligned} J_{0i} &= \bar{\sum}\sum\left\{\frac{g_1(q^2)}{2M}\,\sigma_i P_i + f_1(q^2)\left[1+\frac{\vec{p}\cdot\vec{p'}+i\epsilon_{ilm}\,p'_i p_l \sigma_m}{(2M)^2}\right]\right. \\ &\left. +\frac{f_2(q^2)}{(2M)^2}\,\sigma_l q_l \sigma_m q_m\right\}\left\{g_1(q^2)\,\left[\vec{\sigma}_j+\frac{(\vec{\sigma}\cdot\vec{p'})\sigma_j(\vec{\sigma}\cdot\vec{p})}{(2M)^2}\right]+\frac{f_1(q^2)}{2M}\right. \\ &\left.\left[P_j - i\epsilon_{jl'm'}\,q_{l'}\sigma_{m'}\right] - i\frac{f_2(q^2)}{2M}\,\epsilon_{jl'm'}\,\sigma_{l'}q_{m'}\right\}. \end{aligned} \quad (14.112)$$

Neglecting all the terms with $O(1/M^3)$ or higher powers and using trace relations, we get

$$\begin{aligned} J_{0i} &= 2\left[\frac{g_1^2(q^2)}{2M}\delta_{ij}P_i + \frac{(f_1(q^2))^2}{2M}P_j\right] \\ &= 2\frac{g_1^2(q^2)}{2M}\left[(\delta_{ij}-\hat{q}_i\hat{q}_j)+\hat{q}_i\hat{q}_j\right](2p_i+q_i) + 2\frac{(f_1(q^2))^2}{2M}(2p_i+q_i). \end{aligned} \quad (14.113)$$

Similarly, we find J_{ij} as follows

$$\begin{aligned} J_{ij} &= \bar{\sum}\sum\left\{g_1(q^2)\,\left[\vec{\sigma}_i+\frac{(\vec{\sigma}\cdot\vec{p'})\sigma_i(\vec{\sigma}\cdot\vec{p})}{(2M)^2}\right]+\frac{f_1(q^2)}{2M}\,\left[P_i - i\epsilon_{ilm}\,q_l\sigma_m\right]\right. \\ &\left. -i\frac{f_2(q^2)}{2M}\,\epsilon_{ilm}\,\sigma_l q_m\right\}\times\left\{g_1(q^2)\,\left[\vec{\sigma}_j+\frac{(\vec{\sigma}\cdot\vec{p'})\sigma_j(\vec{\sigma}\cdot\vec{p})}{(2M)^2}\right]+\frac{f_1(q^2)}{2M}\right. \\ &\left.\left[P_j - i\epsilon_{jl'm'}\,q_{l'}\sigma_{m'}\right] - i\frac{f_2(q^2)}{2M}\,\epsilon_{jl'm'}\,\sigma_{l'}q_{m'}\right\}. \end{aligned} \quad (14.114)$$

Neglecting the terms with $1/(2M)^3$, $1/(2M)^4$ or higher powers and using the trace relations given in Appendix C, we get

$$\begin{aligned} J_{ij} &= 2\left\{g_1^2(q^2)\left[(\delta_{ij}-\hat{q}_i\hat{q}_j)+\hat{q}_i\hat{q}_j\right] + \left(\frac{f_1(q^2)}{2M}\right)^2 P_iP_j + 2\frac{f_1(q^2)f_2(q^2)}{(2M)^2}\right. \\ &\left. |\vec{q}|^2\,(\delta_{ij}-\hat{q}_i\hat{q}_j) - |\vec{q}|^2\left(\frac{f_2(q^2)}{2M}\right)^2(\delta_{ij}-\hat{q}_i\hat{q}_j)\right\}. \end{aligned} \quad (14.115)$$

Now the leading term $g_1^2(q^2)\delta_{ij}$ is split between the longitudinal and transverse components as

$$g_1^2(q^2)\delta_{ij}\mathrm{Im}U \to g_1^2(q^2)\left[\hat{q}_i\hat{q}_j + (\delta_{ij}-\hat{q}_i\hat{q}_j)\right]\mathrm{Im}U. \quad (14.116)$$

https://doi.org/10.1017/9781108489065.015 Published online by Cambridge University Press

The RPA response of this term after summing the higher order diagrams like Figure 14.8 is modified and given by J_{ij}^{RPA}:

$$J_{ij} \rightarrow J_{ij}^{RPA} = g_1^2(q^2)\mathrm{Im}\, U \left[\frac{\hat{q}_i\hat{q}_j}{|1-UV_l|^2} + \frac{\delta_{ij}-\hat{q}_i\hat{q}_j}{|1-UV_t|^2}\right], \tag{14.117}$$

Taking $\vec{q}$ along the z direction, Eq. (14.117), implies that the $g_1^2(q^2)\delta_{ij}$ contribution to the transverse (xx, yy) and longitudinal (zz) components of the hadronic tensor gets renormalized by factors $1/|1-UV_l|^2$ and $1/|1-UV_t|^2$, respectively.

The final expressions for the hadronic tensors with RPA correlations are expressed as:

$$\begin{aligned}\frac{J_{00}^{RPA}}{M^2} &= \left(f_1(q^2)\right)^2\left[\left(\frac{E(\vec{p})}{M}\right)^2 + \left(\frac{q_0E(\vec{p})+q^2/4}{M^2}\right)\right] - \frac{q^2}{M^2}\left(\frac{f_2(q^2)}{2}\right)^2 \\ &\left[\frac{\vec{p}^2+q_0E(\vec{p})+q_0^2/4}{M^2}+\frac{q_0^2}{q^2}\right] - \frac{1}{2}\left(f_1(q^2)f_2(q^2)\right)\left(\frac{|\vec{q}|}{M}\right)^2 \\ &+g_1^2(q^2)\left[\frac{\vec{p}^2+q_0E(\vec{p})+q^2/4}{M^2} - U_L\left(\frac{q_0^2}{m_\pi^2-q^2}\right)\left(\frac{q^2}{m_\pi^2-q^2}\right)\right].\end{aligned} \tag{14.118}$$

$$\begin{aligned}\frac{J_{0z}^{RPA}}{M^2} &= \frac{1}{2}\left(f_1(q^2)\right)^2\left[\frac{E(\vec{p})}{M}\left(\frac{2p_z+|\vec{q}|}{M}\right)+\frac{q_op_z}{M^2}\right] - \frac{1}{2}\frac{q^2}{M^2}\left(\frac{f_2(q^2)}{2}\right)^2 \\ &\left[\frac{E(\vec{p})}{M}\left(\frac{2p_z+|\vec{q}|}{M}\right)+\frac{2q_0|\vec{q}|}{q^2}+\frac{q_0\left(2p_z+|\vec{q}|\right)}{2M^2}\right] - \frac{1}{2}\left(f_1(q^2)f_2(q^2)\right) \\ &\left[\frac{q_0|\vec{q}|}{M^2}\right] + g_1^2(q^2)\left[U_L\frac{E(\vec{p})}{M}\left(\frac{2p_z+|\vec{q}|}{2M}\right)+\frac{q_op_z}{2M^2} - U_L\left(\frac{q_0|\vec{q}|}{m_\pi^2-q^2}\right)\right. \\ &\left.\left(\frac{q^2}{m_\pi^2-q^2}\right)\right]\end{aligned} \tag{14.119}$$

$$\begin{aligned}\frac{J_{zz}^{RPA}}{M^2} &= \left(f_1(q^2)\right)^2\left[\frac{p_z^2+|\vec{q}|p_z-q^2/4}{M^2}\right] - \frac{1}{4}\frac{q^2}{M^2}\left(\frac{f_2(q^2)}{2}\right)^2\left[\left(\frac{2p_z+|\vec{q}|}{M}\right)^2\right. \\ &\left.+\frac{q_0^2}{q^2}\right] - \frac{1}{2}\left(f_1(q^2)f_2(q^2)\right)\left(\frac{q_0}{M}\right)^2 + g_1^2(q^2)\left[U_L + \frac{p_z^2+|\vec{q}|p_z-q^2/4}{M^2}\right. \\ &\left.-U_L\left(\frac{|\vec{q}|}{m_\pi^2-q^2}\right)\left(\frac{q^2}{m_\pi^2-q^2}\right)\right].\end{aligned} \tag{14.120}$$

$$\begin{aligned}\frac{J_{RPA}^{xx}}{M^2} &= \left(f_1(q^2)\right)^2\left[\frac{p_x^2-q^2/4}{M^2}\right] - \frac{q^2}{M^2}\left(\frac{f_2(q^2)}{2}\right)^2\left[U_T+\frac{p_x^2}{M^2}\right] \\ &-\frac{1}{2}\left(f_1(q^2)f_2(q^2)\right)U_T\left(\frac{q^2}{M^2}\right) + g_1^2(q^2)\left[U_L+\frac{p_x^2-q^2/4}{M^2}\right].\end{aligned} \tag{14.121}$$

https://doi.org/10.1017/9781108489065.015 Published online by Cambridge University Press

$$\frac{J^{RPA}_{xy}}{M^2} = ig_1(q^2)\left[f_1(q^2)+f_2(q^2)\right]\left[\frac{q_0 p_z}{M^2} - U_T\frac{|\vec{q}|E(\vec{p})}{M^2}\right]. \quad (14.122)$$

With the incorporation of these nuclear medium effects, the expression for the total scattering cross section $\sigma(E_\nu)$ is given by Eq.(14.92) with $J^{\mu\nu}$ replaced by $J^{\mu\nu}_{RPA}$(defined in Eq. (14.117)), that is,

$$\sigma(E_\nu) = -\frac{G_F^2 a^2}{32\pi}\int_{r_{\min}}^{r_{\max}} r^2 dr \int_{k'_{\min}}^{k'_{\max}} k'^2 dk' \int_{-1}^{+1} d(\cos\theta)\frac{1}{E_{\nu_l}E_l} L_{\mu\nu}J^{\mu\nu}_{RPA} \times \mathrm{Im}U_N(q_0^{\nu(\bar{\nu})} - V_c(r)), \quad (14.123)$$

where $J^{\mu\nu}_{RPA}$ is the hadronic tensor with its various components modified due to long range correlation effects treated in RPA. In Eq. (14.123), $a = \cos\theta_c$ for the charged current reaction. For neutral current reactions, $a = 1$ with the Lindhard function is calculated without the Coulomb potential $V_c(r)$.

14.6 Cross Sections and Effect of Nuclear Medium

We show the results for the (anti)neutrino–nucleus cross sections in ^{12}C, ^{40}Ar, ^{56}Fe, and ^{208}Pb nuclei as a function of energy in Figure 14.9, by plotting the ratio of scattering cross section per interacting nucleon to the scattering cross section on the free nucleon target. The results are obtained using the local Fermi gas (LFG) model and the local Fermi gas model with RPA effect (LFG+RPA). A large reduction in the cross section at low energies can be seen which increases with the nucleon number A. In the region of low energy, the reduction is larger in the case of $\nu_\mu(\bar{\nu}_\mu)$ induced reactions in comparison to $\nu_e(\bar{\nu}_e)$ reactions which is mainly due to the threshold effects. The reduction in the cross sections due to nuclear medium effects for the neutrino and antineutrino reactions has similar energy dependence except that it is slightly larger in the case of antineutrino reactions.

In Figure 14.10, we have shown the results of the effect of the nuclear medium in the lepton momentum distribution $\frac{d\sigma}{dp_\mu}$ for the ν_μ and $\bar{\nu}_\mu$ induced charged current quasielastic processes at $E_\nu = 1$ GeV. We find that when the nuclear medium effects are taken into account, there is a reduction as well as shift in the peak region toward the lower value of lepton momentum. This reduction in $\frac{d\sigma}{dp_\mu}$ when calculated in the local Fermi gas model without the RPA correlation effects as compared to the cross section calculated without the nuclear medium effects is around 10% in the peak region of the lepton momentum distribution, which further reduces by around 30% when RPA effects are also taken into account. In the case of antineutrinos, the reduction in $\frac{d\sigma}{dp_\mu}$ in the local Fermi gas model is around 30% which further reduces by 30% when RPA effects are also taken into account.

We show the results for the nuclear medium effects in the total cross sections σ for ^{40}Ar and compare them with the calculations done in the other variants of the Fermi gas model (Smith and Moniz [657], Llewellyn Smith [294] and Gaisser and O'Connell [658]) in Figure 14.11 by plotting fractional difference $\delta\sigma_{\text{model}}(= \frac{\sigma_{\text{free}}-\sigma_{\text{model}}}{\sigma_{\text{free}}})$. Here σ_{free} stands for the (anti)neutrino induced interaction cross section on free nucleon targets and σ_{model} stands for the (anti)neutrino

https://doi.org/10.1017/9781108489065.015 Published online by Cambridge University Press

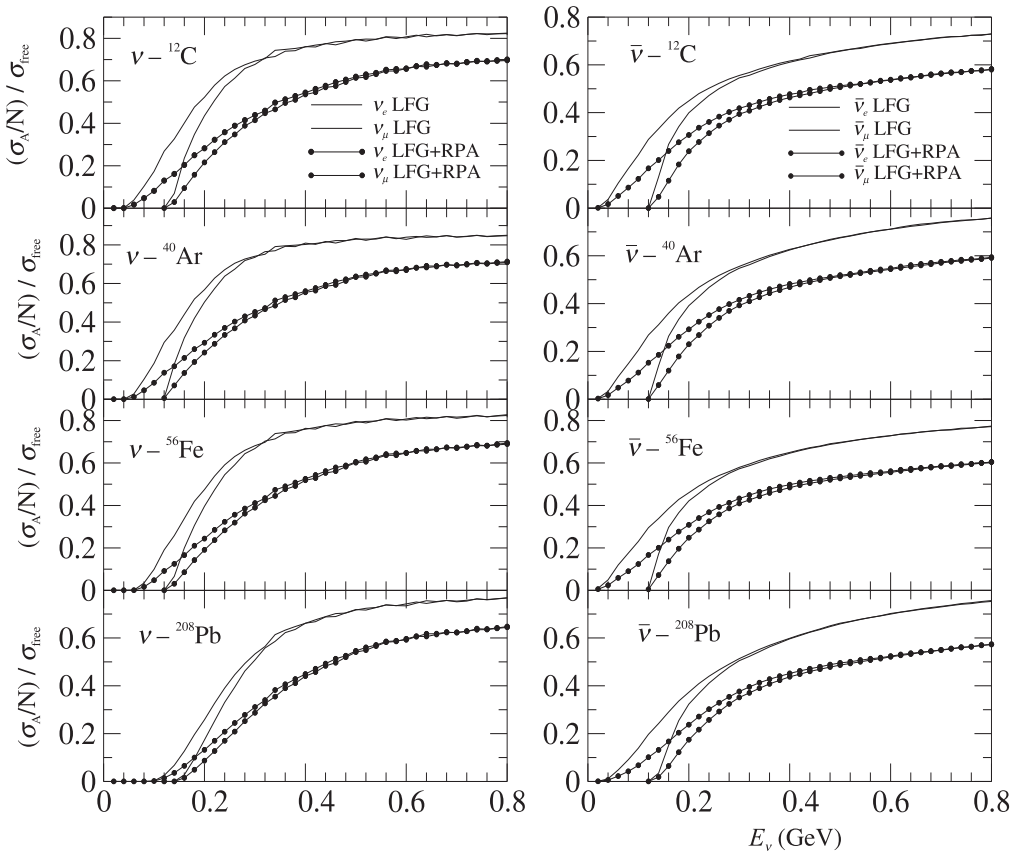

Figure 14.9 Ratio $\frac{\sigma_A/N}{\sigma_{free}}$ vs. E_ν, for neutrino (left panel) and antineutrino (right panel) induced processes in ^{12}C, ^{40}Ar, ^{56}Fe, and ^{208}Pb. The solid (dashed) line represent cross sections obtained from electron (muon) type neutrino and antineutrino beams. For neutrino induced processes, $N = A - Z$ is the neutron number and for antineutrino induced processes, $N = Z$ is the proton number. σ_A is the cross section for the nuclear target and has been evaluated using the local Fermi gas model and LFG with RPA effect (LFG+RPA). σ_{free} is the cross section for the free nucleon case.

induced interaction cross section for the nucleons bound inside the nucleus. The difference in the results for neutrino and antineutrino cross sections is mainly due to the interference terms between the vector and the axial vector contributions which come with an opposite sign for neutrino and antineutrino. In the case of LFG with RPA effects, the effect of renormalization is large and this suppresses the terms with f_2 and g_1, which results in a large change in neutrino as compared to antineutrino cross section. We find appreciable difference in the results when various nuclear models are used.

There are two types of corrections which appear when lepton mass $m_l (l = e, \mu)$ is taken into account in the cross section calculations for the reaction $\nu_l(\bar{\nu}_l) + N \rightarrow l^-(l^+) + N'$, $(N, N' = n, p)$ which can be classified as kinematical and dynamical. The kinematical effects arise due to $E_l \neq |\vec{k}'|$ in the presence of m_l and the minimum and maximum values of

https://doi.org/10.1017/9781108489065.015 Published online by Cambridge University Press

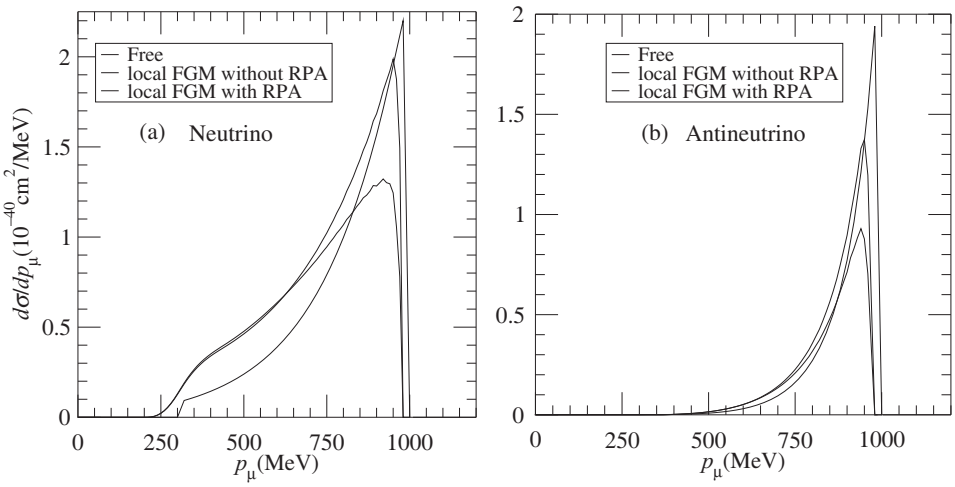

Figure 14.10 $\frac{d\sigma}{dp_\mu}$ vs. p_μ for the $\nu_\mu(\bar{\nu}_\mu)$ induced reactions on ^{12}C target at $E_\nu = 1$ GeV. The short dashed line is the result for the free case, the long dashed (solid) line is the result obtained using local Fermi gas model without (with) RPA.

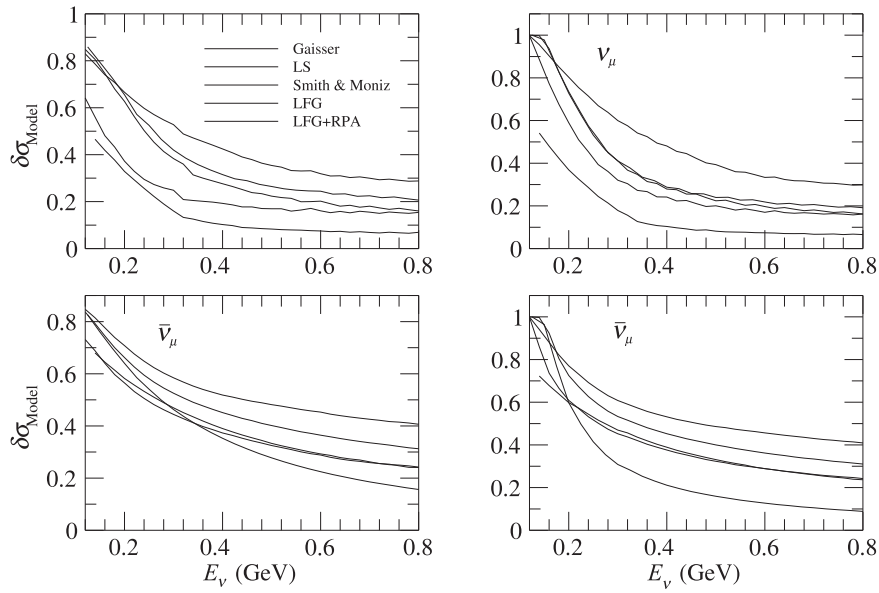

Figure 14.11 The fractional suppression in cross section $\delta\sigma_{\rm model}(=\frac{\sigma_{\rm free}-\sigma_{\rm model}}{\sigma_{\rm free}})$ vs. E_ν, where $\sigma_{\rm free}$ is the cross section obtained for free nucleons and $\sigma_{\rm model}$ is the interacting nucleon cross section in ^{40}Ar obtained by using different nuclear models. The results are presented for the cross sections obtained from different models of Fermi gas (σ_{Model}) viz. Smith and Moniz [657](dashed dotted line), Llewellyn Smith [294](dashed line), Gaisser O' Connell [658](solid line), and with (double dashed dotted line) and without RPA (dashed double dotted line) effect using the local Fermi gas model. The top panel is for neutrino and the bottom panel is for antineutrino induced processes.

https://doi.org/10.1017/9781108489065.015 Published online by Cambridge University Press

four-momentum transfer squared ($Q^2 = -q^2 \geq 0$), that is, $Q^2_{\rm min}$ and $Q^2_{\rm max}$ gets modified, affecting the calculations of total cross sections. These effects are negligible for highly relativistic leptons but could become important at low energies near the threshold energy, especially for muons. On the other hand, dynamical corrections arise as additional terms proportional to $\frac{m_l^2}{M^2}$ in the existing contribution of vector and axial vector form factors as well as new contributions due to induced pseudoscalar and other form factors associated with second class currents come into play. In fact, all the contributions from the pseudoscalar form factor $g_3(q^2)$ and the second class vector form factor $f_3(q^2)$ are proportional to $\frac{m_l^2}{M^2}$, while the contribution from the second class axial vector form factor $g_3(q^2)$ is proportional either to $\frac{m_l^2}{M^2}$ or $\frac{q^2}{M^2}$ or both.

To study the lepton mass dependence on $\nu_e(\bar{\nu}_e)$ and $\nu_\mu(\bar{\nu}_\mu)$ induced scattering cross sections in free nucleons as well as in nuclear targets, we define $\Delta_I = \frac{\sigma_{\nu_e(\bar{\nu}_e)} - \sigma_{\nu_\mu(\bar{\nu}_\mu)}}{\sigma_{\nu_e(\bar{\nu}_e)}}$ for the (anti)neutrino induced reaction in ^{12}C and ^{40}Ar nuclear targets, where $I = i, ii, iii$, which respectively stands for the cross sections obtained in (i) the free (anti)neutrino–nucleon case, (ii) the local Fermi gas model (LFG) and (iii) the local Fermi gas model with RPA effect(LFG+RPA). The results are presented in Figure 14.12, which show that the differences in the electron and muon production cross sections for $\nu_l(\bar{\nu}_l)$ induced reactions on ^{12}C targets are appreciable at low energies $E_\nu < 0.4$ GeV.

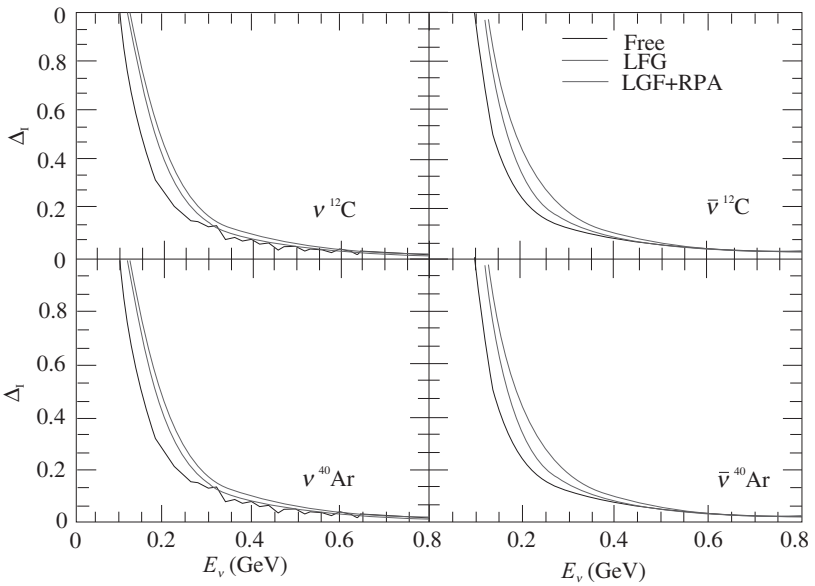

Figure 14.12 $\Delta_I = \frac{\sigma_{\nu_e(\bar{\nu}_e)} - \sigma_{\nu_\mu(\bar{\nu}_\mu)}}{\sigma_{\nu_e(\bar{\nu}_e)}}$ for neutrino (left panel) and antineutrino (right panel) induced processes in ^{12}C and ^{40}Ar targets. Here, I stands for the results of the cross sections obtained (i) for the free nucleon case (solid line), (ii) in the local Fermi gas model (dashed line) and (iii) for LFG with RPA effect (dashed dotted line).

https://doi.org/10.1017/9781108489065.015 Published online by Cambridge University Press

14.7 Nuclear Medium Effects in Neutrino Oscillation Experiments

The discovery of neutrino oscillations with solar, reactor, atmospheric, and accelerator neutrinos has motivated many experiments on neutrino–nucleus cross section measurements in the entire region of low and intermediate energies. These cross sections in this energy region are significantly affected by the nuclear medium effects and the q^2 dependence of the electroweak form factors of the nucleon specially in the region of a few hundred MeV to few GeV. While the weak vector form factors $f_i(q^2)$ $(i = 1, 2)$ are well determined from the electron-nucleus scattering. The study of the nuclear medium effects on the axial vector form factor $g_i(q^2)$ was mainly confined to the study of $g_1(0)$ and $g_3(0)$ leading to the quenching of $g_1(0)$ and enhancement of $g_3(0)$ in nuclei due to various nuclear medium effects. The q^2 dependence of the axial vector form factors is parameterized in terms of the axial mass M_A in the context of dipole parameterization of $g_1(q^2)$ (Chapter 10). The q^2 dependence of $g_3(q^2)$ is related to $g_1(q^2)$ through PCAC. The effect of the nuclear medium on M_A was neglected at the beginning and was first studied by Singh and Oset [639] emphasizing the need for better experiments in the region of low q^2. The present generation of neutrino oscillation experiments done in the energy region of ~ 1 GeV in nuclei are best suited for studying the effect of the nuclear medium on M_A.

The early measurements of M_A were made from the neutrino scattering experiments on deuterium and nuclear targets. The deuterium measurements for M_A had better precision and were in agreement with the measurements made from the threshold electroproduction of pions. The nuclear measurements of M_A had large experimental uncertainties and were in general smaller than the value determined from the deuterium experiment; however, they were in agreement within the experimental error bars. A world average value of $M_A = 1.026$ GeV was generally used in many studies [443].

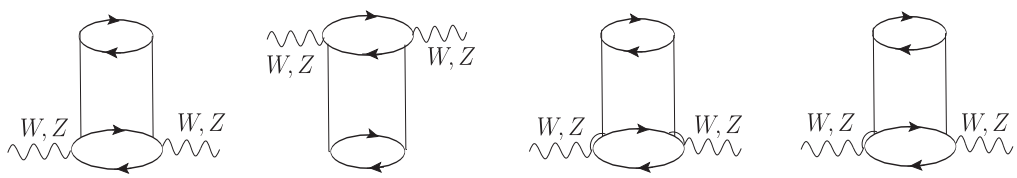

Figure 14.13 Diagrams showing some typical $2p - 2h$ contributions arising due to the $N - N$ and $N - \Delta$ correlations. Solid (dashed) lines denote nucleon (pion) propagators. Double lines represent $\Delta(1232)$ propagators. Arrows pointing to the right (left) denote particle (hole) states.

In 2009, the MiniBooNE collaboration reported new measurements on the charge changing quasielastic process using a high statistics sample of ν_μ interactions in ^{12}C with average energy $\langle E_\nu \rangle = 750$ MeV [435], which were considerably higher than the theoretical predictions. Subsequently, the results on the double differential cross sections $\frac{d^2\sigma}{d\cos\theta dE'}$ were also presented which confirmed the findings of the cross section measurements. These results could be explained with $M_A = 1.35 \pm 0.17$ GeV, which was considerably higher than the world average. This is known as the MiniBooNE puzzle.

https://doi.org/10.1017/9781108489065.015 Published online by Cambridge University Press

The MiniBooNE puzzle initiated an extensive debate on the nuclear medium effects in (anti)neutrino nucleus scattering. Since the ^{12}C nucleus used in many neutrino oscillation experiments is one of the best known nucleus theoretically as well as experimentally, from the study of electron nucleus scattering regarding its wave function, it was very difficult to explain the discrepancy in the measurement of neutrino cross sections at MiniBooNE. It was attributed to other nuclear effects beyond impulse approximation due to MEC and nucleon–nucleon correlations or FSI effects leading to quasielastic-like events.

Such effects have been discussed earlier in electron scattering and applied to neutrino scattering by Martini et al. [690, 691] and later by Nieves et al. [692] and many others [693, 694]. Some of these effects beyond the impulse approximation were also included in the works of Valencia and Aligarh groups [659, 660, 661, 662, 663, 664, 665, 666, 667, 668] done on the local Fermi gas model through long range RPA correlations. However, the new results from MiniBooNE were too high to be explained by these approaches. Various calculations done earlier in the microscopic model including the initial state interactions through the nucleon spectral functions in the nucleus were also found to underestimate the cross section measurements from MiniBooNE. A summary of these theoretical calculations along with the results of MiniBooNE is given in Ref. [678].

After the experimental results of MiniBooNE, it was emphasized by Martini et al. and Nieves et al. that there are additional contributions coming from MEC and nucleon–nucleon correlation effects, which are not included in most of the earlier calculations. In earlier treatments of including such effects, the diagrams corresponding to Figure 14.13 were taken into consideration while the diagrams corresponding to Figure 14.14 and the other diagrams where W and Z bosons interact directly with the non-nucleonic degrees of freedom in the nucleus were not fully incorporated.

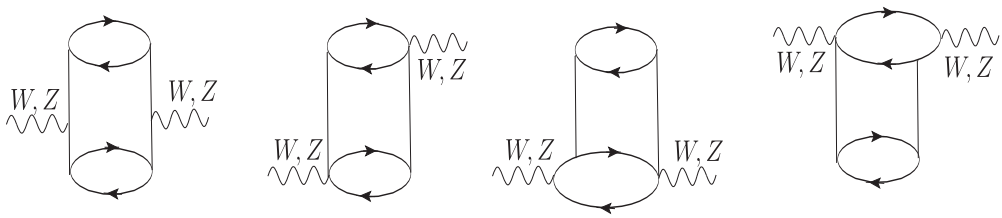

Figure 14.14 Diagrams showing some typical $2p-2h$ contributions arising due to the meson exchange. Solid (dashed) lines denote nucleon (pion) propagators. Arrows pointing to the right (left) denote particle (hole) states.

The elaborate calculations done by Martini [691] in the microscopic model and Nieves et al. [661] in the relativistic Fermi gas model included most of the diagrams and showed that the enhancement in the cross sections in MiniBooNE comes from the contribution from the $2p-2h$ excitations shown in Figures 14.13 and 14.14, and its interference with the $1p-1h$ contribution. Once these contributions are included, the results from MiniBooNE can be explained using the value of $M_A = 1.049$ GeV, consistent with the world average value of M_A as shown in Figure 14.15.

https://doi.org/10.1017/9781108489065.015 Published online by Cambridge University Press

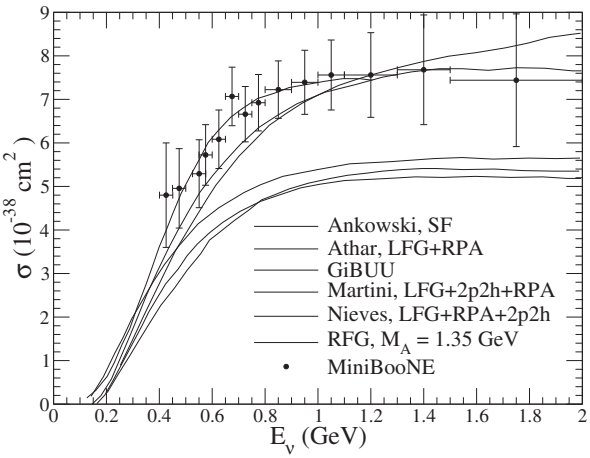

Figure 14.15 "Quasielastic-like" ν_μ-^{12}C cross sections measured by MiniBooNE [435] compared to Martini et al. calculations. The figure is taken from Ref. [356].

In Figure 14.16, the neutrino and antineutrino differential cross section $d\sigma/dQ^2$, measured in Refs. [435] and [695] and as calculated in Refs. [690] and [691] are presented. It may be observed that the inclusion of $2p-2h$ and the meson exchange currents contribution results in a better description of data in comparison to QE results without these nuclear effects.

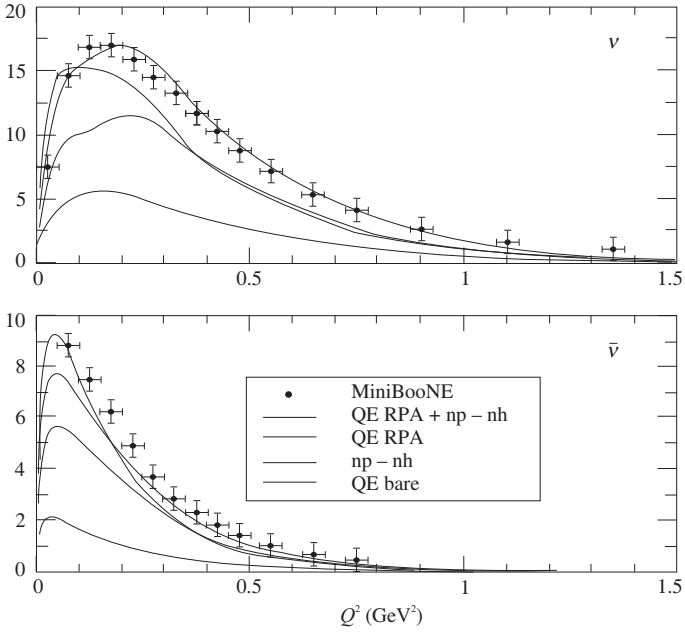

Figure 14.16 MiniBooNE flux-integrated differential cross sections $d\sigma/dQ^2$ vs. Q^2 in units of 10^{-39} cm^2/GeV^2 for neutrino (upper panels) and antineutrino (lower panels) CCQE-like scattering on carbon. The experimental MiniBooNE points are taken from [435] and [695]. The theoretical results are the ones of Refs. [690] and [691].

https://doi.org/10.1017/9781108489065.015 Published online by Cambridge University Press

It has to be emphasized that the nuclear medium effects are very important in the region of intermediate energies ($E_\nu \sim 1$ GeV) relevant for most neutrino oscillation experiments being done at present and planned in the future.

https://doi.org/10.1017/9781108489065.015 Published online by Cambridge University Press